

Heat pipe-cooled reactors: A comprehensive review of evolution, challenges, research status, and outlook

Zeqin Zhang^{ID}, Zhipeng Zhang, Chenglong Wang^{*}^{ID}, Kailun Guo, Wenxi Tian, Guanghui Su, Suizheng Qiu

Shaanxi Key Laboratory of Advanced Nuclear Energy and Technology, School of Nuclear Science and Technology, Xi'an Jiaotong University, Xi'an, 710049, China



ARTICLE INFO

Keywords:

Heat pipe-cooled reactor
Heat pipe
Energy solution
Advanced nuclear system
Small modular reactor
Sustainable nuclear energy
Off-grid power supply

ABSTRACT

Amid the growing demand for sustainable and efficient energy solutions, Heat Pipe-Cooled Reactors (HPRs) have emerged as a promising innovation in nuclear energy, offering inherent safety, modularity, and high energy density. However, despite significant progress in HPR research, critical challenges still remain in system design, fuel enrichment, material performance, and heat transfer limitations. This review aims to provide a comprehensive overview of HPR development, systematically summarizing its evolution, key characteristics, and current research advances. First, a detailed timeline of HPR technology evolution is outlined to contextualize its current status. The concept and design principles of HPRs are subsequently introduced, with an in-depth analysis of challenges in core configurations, high-temperature heat pipes design, and energy conversion systems. Moreover, the latest advancements of HPR-related studies are reviewed, including fundamental studies, technological improvement, innovation designs and experimental validations. Finally, future research directions are identified, focusing on enhancing reliability, optimizing designs, and broadening application areas to address existing challenges and unlock the full potential of HPRs.

Abbreviations

AFSPS	Affordable Fission Surface Power System
AMTEC	Alkali Metal Thermal-to-Electric Converter
BASE	Beta Alumina Solid Electrolyte
CFD	Computational Fluid Dynamics
CAEP	China Academy of Engineering Physics
CNRS	Centre National de la Recherche Scientifique
CNSC	Canadian Nuclear Safety Commission
DUFF	Demonstration Using Flattop Fissions
FSM	Frozen Start-up Model
FPSE	Free-Piston Stirling Engine
HEU	High-Enriched Uranium
HFM	Heat and Flow Model
HPR	Heat Pipe-cooled Reactor
HTHP	High-Temperature Heat Pipe
HOMER	Heat pipe-Operated Mars Exploration Reactor
HP-STMCs	Heat Pipe-Segmented Thermoelectric Module Converters
IAE	Institute of Atomic Energy
KRUSTY	Kilopower Reactor Using Stirling TechnologY
LM	Lumped Model
LBM	Lattice Boltzmann Method
LEU	Low-Enriched Uranium

(continued)

AFSPS	Affordable Fission Surface Power System
LMP	Larson-Miller Parameter
LVI	Liquid-Vapor Interface
LANL	Los Alamos National Laboratory
LOCA	Loss of Coolant Accident
LOFA	Loss of Flow Accident
MHD	Magnetohydrodynamic
MIT	Massachusetts Institute of Technology
MPC	Model Predictive Control
MSR	Martian Surface Reactor
MNPS	Mobile Nuclear Power System
NTM	Network Thermodynamics Model
NASA	National Aeronautics and Space Administration
NNSS	Nevada National Security Site
NUSTER	NUclear Silent Thermal-Electrical Reactor
ODS	Oxide Dispersion Strengthened steel
ORNL	Oak Ridge National Laboratory
PSV	Power Supply Vehicle
RTC	Reactivity Temperature Coefficient
SS	Stainless Steel
SCO ₂	Supercritical Carbon-dioxide
SNL	Sandia National Laboratory

(continued on next column)

(continued on next page)

* Corresponding author.

E-mail address: chlwang@mail.xjtu.edu.cn (C. Wang).

(continued)

AFSPS	Affordable Fission Surface Power System
SMR	Small modular reactor
STEG	Segmented Thermoelectric Generator
SAIRS	Scalable AMTEC Integrated Reactor Space Power System
SINAP	Shanghai Institute of Applied Physics
SUPERHERO	SUPERcritical carbon dioxide cycle-HEat pipe ReactOr power system
TEG	Thermoelectric Generator
TIC	Thermionic Converter
TPV	Thermophotovoltaic
TZM	Titanium-Zirconium-Molybdenum alloy
TIPV	Thermionic-Photovoltaic
TRISO	Tri-Structural Isotropic particle fuel
UNM	University of New Mexico
UUV	Unmanned Underwater Vehicle
UIUC	University of Illinois at Urbana-Champaign
XJTU	Xi'an Jiaotong University

1. Introduction

The growing global demand for dependable and sustainable energy solutions has sparked a pursuit of clean and environmentally friendly power sources. Nuclear energy, recognized for its significance as a clean and sustainable energy source, has gained acknowledgment at COP28 [1]. Over the past 60 years, centralized nuclear energy supply has dominated the market, mainly via large-scale commercial nuclear power plants. With advancements in energy structures and the adoption of Generation-IV reactor technology, distributed nuclear energy supply is increasingly showcasing its advantages, particularly in regions where traditional fossil fuels are diminishing. In the future nuclear energy

market, miniaturization, off-grid capabilities, and modularization are expected to play increasingly significant roles. In response, micro-reactors have emerged as an innovative small-scale nuclear energy solution, offering exceptional miniaturization, cost-effectiveness, and enhanced safety. These reactors, classified as Small Modular Reactors (SMRs) [2], typically produce less than 20 MWe [3].

The Heat Pipe-cooled Reactor (HPR) is a unique type of SMR that relies entirely on in-core heat pipes to passively transfer heat from the core to the power generation system. This design eliminates the need for primary loop cooling and pump systems, significantly simplifying the core design. Typically, the coolant is replaced with a metal or alloy matrix, making this type of reactor also known as a solid-state reactor. With its fully passive design concept, the HPR is regarded as inherently safe, capable of avoiding single-point failures and preventing both Loss of Coolant Accidents (LOCA) and Loss of Flow Accidents (LOFA) [4]. Based on these advantages, HPRs are widely adopted in concept designs requiring simplicity, compactness, long-duration endurance, high reliability, and unmanned operation. These applications primarily include deep-sea [5], deep-space [6], and land-based [7] scenarios. Depending on the application scenario, HPRs can be adapted to various energy conversion systems, including static and dynamic conversion forms. The former typically generates electricity through direct thermoelectric conversion, achieving lower efficiency (~15 %), making it suitable for silent, low-power applications. The latter typically converts thermal energy into various forms of mechanical energy, which is converted into electrical energy, achieving higher efficiency (~40 %) and suitable for high-power applications.

Regarding energy supply capability, HPRs achieve almost 100 % capacity factor, providing significantly greater stability compared to traditional renewable energy sources. A mobile HPR facility requires

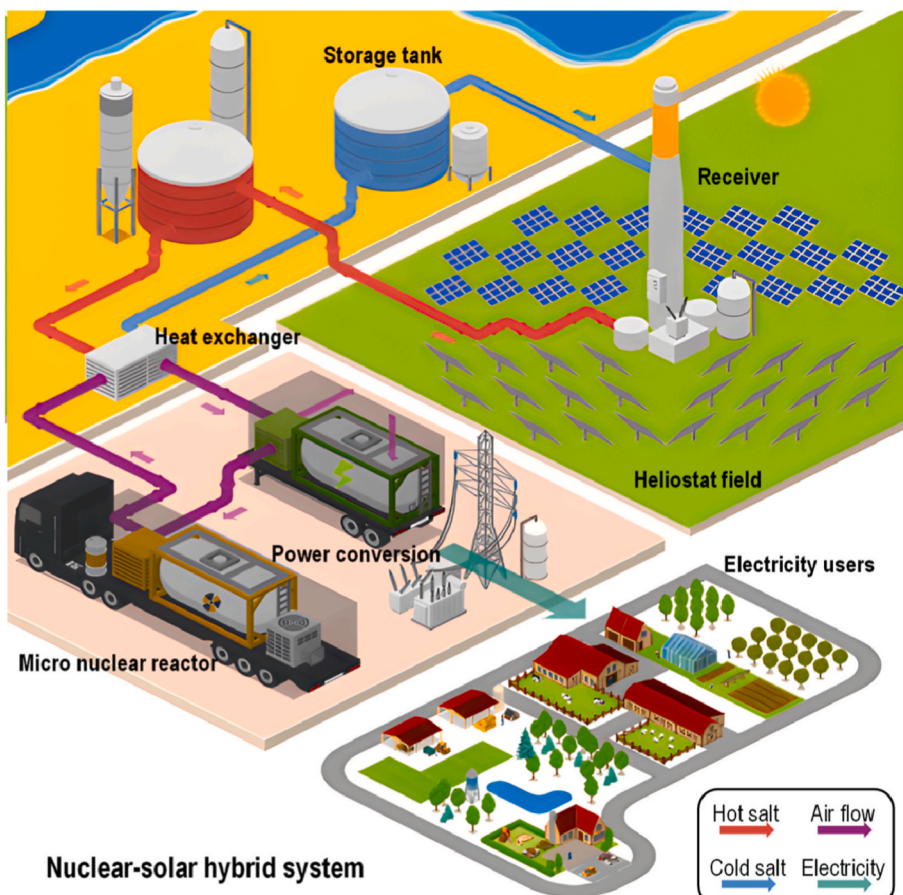


Fig. 1. Schematic diagram of HPR-solar hybrid energy system [9].

only 1.67 % of the land needed for solar installations and 0.29 % for wind installations to supply equivalent power [8]. Moreover, for remote off-grid power supply, the HPR can integrate with other energy sources, such as solar systems (Fig. 1), improving efficiency, shortening the payback period, and enhancing economic competitiveness in the energy market [9]. These benefits have driven a rapid growth in HPR research in recent years.

Currently, HPR has transitioned from the conceptual design stage to practical engineering applications. Institutions such as Los Alamos National Laboratory (LANL) have conducted a series of key technological studies on HPR [10], demonstrating its feasibility in terms of inherent safety [11], energy conversion adaptability [12], and prototype testing [13]. Furthermore, the land-based commercial solutions, such as eVinci [14], indicates that HPR will significantly contribute to the distributed nuclear power supply market. However, at the current stage of HPR research, significant gaps remain in areas such as neutronics, thermal hydraulics, and mechanics. Additionally, the technological maturity for processing and manufacturing, integrated assembly, deployment, and decommissioning remains insufficient.

To address the current gaps in HPR research, several review studies have summarized the technological advancements in this field. Yan et al. [15] provided an in-depth overview of micro HPRs, focusing on their fundamental principles, neutronics and thermal-hydraulic characteristics, thermal performance, and potential applications, laying a crucial foundation for subsequent research. More recently, Bo et al. [16] reviewed key progress in HPR technology, with an emphasis on advancements in modeling, experimental validation, and safety analysis. These reviews offer detailed and in-depth insights into key technical aspects, contributing valuable perspectives on the evolution and feasibility of HPR systems.

To further enhance a comprehensive understanding of HPR technology, this review aims to provide a broader system-level perspective by systematically examining the evolution, key characteristics, major challenges, and recent advancements in HPR technology. The novelty of this work lies in its critical evaluation of the strengths and weaknesses of existing studies from a system-level, rather than merely summarizing and listing findings, which has not been vividly explored in previous reviews. Accordingly, this review focuses on: (i) the historical evolution and key milestones of HPR technology, (ii) the primary characteristics of HPR systems and the associated challenges, and (iii) the latest advancements in HPR research, including fundamental studies, technological improvements, innovative designs, and experimental validations. It is hoped that this review will serve as a helpful resource for researchers and engineers in the field.

2. Evolution and development of HPR technology

Although HPR is currently a popular concept in the energy sector, its technology has been under development for 60 years. Understanding the evolution and development of HPR technology is useful for comprehending the opportunities and challenges it faces today. This section provides an overview of the three key stages in the evolution and development of HPR technology.

2.1. Early exploration stage (1960s–1990s)

The research on HPRs originated from space reactor projects [17]. Between 1965 and 1988, heat pipe technology was extensively applied in space reactor designs as heat transfer components in radiative coolers, including SNAP-10A [18], Romashka [19], BUK [20–23], TOPAZ-I [22], and TOPAZ-II [23,24].

As early as the 1960s, LANL proposed to directly cool the reactor core through heat pipes [25]. However, due to limitations in materials and thermoelectric conversion technology at the time, HPRs could not overcome main bottlenecks. Research on HPRs became sparse in the 1990s.

2.2. Active design stage (2001–2014)

Since 2000, the reintroduction of space programs renewed interest in HPRs. NASA's space exploration program roadmap [26,27] identified HPRs as the primary option for the 1–10 kWe nuclear power pathway. In 2001, LANL proposed the Heatpipe-Operated Mars Exploration Reactor (HOMER) design [28,29], establishing a foundation for subsequent designs [30]. Conceptual designs such as SAIRS [31], HP-STMCs [32–35], MSR [36], and MegaPower [37] were subsequently developed, but none of them entered the prototype test stage.

Since 2010, NASA has shifted its focus on simpler, cost-effective engineering projects, rather than complex designs, high costs, and reliance on novel materials [38]. Based on the accumulation from the Prometheus [39] and AFSPS [40] projects, NASA developed Kilopower [38], a reactor design for 1–10 kWe output, which simplifies previous designs, retains their advantages, and allows scalability based on power needs [41].

In 2012, NASA successfully conducted the Demonstration Using Flattop Fissions (DUFF) [11] experiment, marking the first nuclear-loaded test in HPR history and demonstrating the feasibility of the core-heat pipe-Stirling device technology.

2.3. Engineering breakthrough stage (since 2015)

In 2015, NASA started the Kilopower Reactor Using Stirling Technology (KRUSTY) project, marking HPR's transition into the engineering testing phase with system component evaluations (Fig. 2) [12]. By 2017, KRUSTY developed a ground prototype and conducted non-nuclear tests to verify full-power operation and power transient adjustments. In 2018, a nuclear-loaded prototype successfully completed a full-power cycle test at the Nevada National Security Site (NNSS) [13]. In 2020, KRUSTY finalized the thermal critical experiment [42], further validating its feasibility.

The success of KRUSTY has highlighted the advantages and potential of HPRs, gaining widespread recognition. Westinghouse introduced the commercial HPR solution eVinci [14], a semi-automated, transportable small modular power system with capacities up to 15 MWe. In 2021, Westinghouse completed an ultra-long time heat pipe durability testing (Fig. 3) [14], marking an important milestone in the commercialization of HPR [43]. In 2023, Westinghouse submitted a vendor design review pre-application to the Canadian Nuclear Safety Commission (CNSC) for eVinci and plans to build its first demonstration project in Canada.

To date, HPR applications are no longer confined to deep-space missions, with various designs now offering power outputs from kilowatts to megawatts. Table 1 summarizes the major current HPR designs, and Fig. 4 highlights key milestones in HPR development. Despite nuclear-fueled tests marking significant progress, practical application and deployment face substantial challenges, which will be explored in detail in the next section.

3. Key characteristics and associated challenges of HPRs

HPR is a solid-state reactor that transfers fission heat from the core to the energy conversion system using heat pipes (Fig. 5), achieving a design that is simple, efficient, passive, and reliant on non-mechanical cooling. Compared to traditional reactors, HPRs differ significantly in structure, cooling methods, materials, and operating temperature. These distinct characteristics present unique challenges, particularly in the configuration of the core, the design of the heat pipe, and the integration of the energy conversion system. This section will provide an overview from these three perspectives.

3.1. Configuration of reactor core

3.1.1. Spectrum and fuel

The core volume of an HPR is approximately 10 % that of traditional

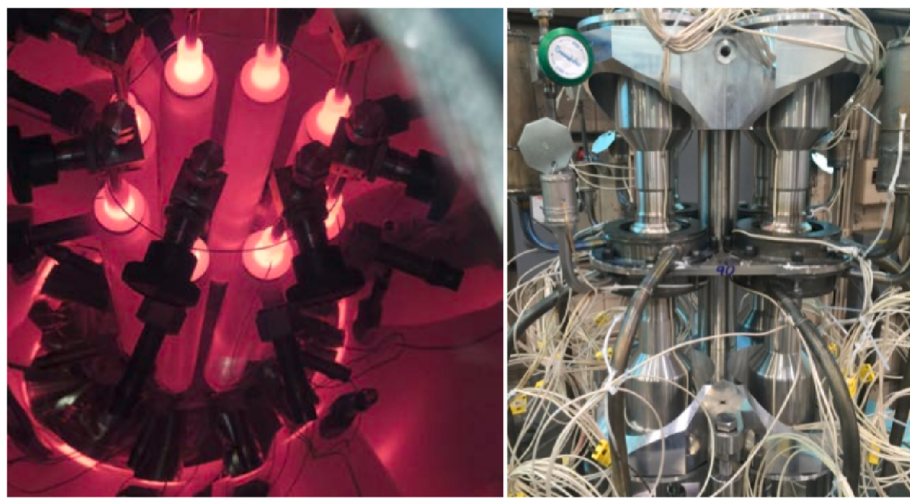


Fig. 2. Core prototype testing (left) and Stirling device testing (right) [12].



Fig. 3. Westinghouse testing platform [14].

commercial reactors. Achieving criticality typically requires a fast neutron spectrum and High-Enriched Uranium (HEU), which reduces core weight [52] but compromises neutron economy [15] and raises concerns about nuclear proliferation [53]. To balance neutron economy and core volume, innovative fuels are required to replace conventional uranium oxide fuel [54].

In addition to UO₂, five other fuel types are considered viable for HPR applications: UN [55], UC [56], UZrH [57], UMo [58], and TRISO (Tri-Structural Isotropic particle fuel) [59]. Each of these fuels has its own advantages and disadvantages, as summarized in Table 2. Considering thermal properties, neutron characteristics, and stability, UN is currently the most widely adopted fuel in HPR designs. Meanwhile, TRISO fuel has achieved breakthrough advancements in high-temperature gas-cooled reactor research [59], making it well-suited for high-temperature applications [60] and offering promising prospects for Low-Enriched Uranium (LEU) deployment in HPRs.

3.1.2. Reflector and shielding

HPRs have significant neutron leakage, necessitating larger reflector and control components [28]. Traditional reflector materials, such as water, heavy water, and borated steel, are not suitable [61]. Potential reflector materials include Be, BeO and graphite [62]. Graphite exhibits high-temperature resistance, its reflectivity, however, is inferior to that of BeO and Be [63]. BeO outperforms Be in neutron performance, properties, and high-temperature performance, making it the optimal

choice for HPRs. The disadvantage is the weight penalty caused by high density.

On the other hand, shielding the intense radiation of an HPR within space and weight constraints is a major challenge. Early space reactors primarily focused on protecting electrical and control systems, employing shadow shielding (Fig. 6) to effectively reduce system weight [43]. However, this approach is not suitable for terrestrial applications due to the increased risk of radiation exposure to personnel. A fully encapsulated core shield, while safer, significantly increases the system's mass [64].

A composite shielding approach, consisting of alternating layers of heavy nuclear materials and hydrogen-containing materials, is currently considered a feasible solution [65]. This configuration provides effective shielding against neutrons and gamma radiation and has been proved to significantly reduce the overall system weight [66].

However, current studies have largely overlooked the possibility of neutrons traveling along the heat pipe cavity and escaping the core. Without additional shielding, the radiation dose at the heat pipe condenser may exceed acceptable limits.

3.2. Design of high-temperature heat pipe (HTHP)

3.2.1. Structure and working fluid

The operating temperature of HPRs exceeds 1000 K, necessitating the use of HTHPs (Fig. 7) [66]. Axially, they can be divided into three

Table 1
Design parameters of HPR concepts.

Parameter	Kilopower	HOMER-15/25	SAIRS	HP-STMCs	MSR-A	MegaPower	eVinci	NUSTER	PSV	MNPS-1000	SUPER HERO	HPCR	micro-MSR
Institution Reference Spectrum Power	LANL [38]	LANL [44,45]	UNM [31]	UNM [32–35]	MIT [36]	LANL [37]	Westinghouse [14]	XJTU [46]	XJTU [47]	CAEP [48]	CAEP [49]	XJTU [50]	SINAP [51]
F 1 kWe	F 3/25 kWe	F 100 kWe	F 110 kWe	F 100	F 5 MWt	E 0.2–15 MWe	F 100 kWt	F 1.08 MWt	F 1 MWe	F 1 MWe	F 3.2 MWt	T 50kWt	F
Efficiency	23.20 %	20 %/26.7 %	18.5%–22.1 %	6.7%–10 %	>10 %	~40 %	~28.6 %	12 %	21.3 %	33.3 %	32 %	31 %	10%–20 %
Heat Pipe Working Fluid	Na	Na/K	Na	Li	Li	Na/K	Na	Na	Na	Li	K	Li	Na
Heat Pipe Arrangement	S	S	S	S	S	D	D	D	D	S	S	S	S
Operating Temperature	1050 K	<1100/880 K	1100–1200 K	1500 K	1800 K	1250/950 K	920 K	1130 K	<1100K	1323 K	1023 K	1750 K	873–973K
Heat Pipe Quantity	8	19/61	60	126	127	1224	876/1224	109	270	216	390	234	37
Refuelling Cycle	10a	5a	5-7a	10-15a	5a	>10a	10a	>5a	>10a	3000d	15a	7a	Unknown
Fuel	UMo	UN/UO ₂	UN	UN	UN/UO ₂	UN/UO ₂	UN/UO ₂	UN/UO ₂	UN	UN	UN	UN	LiF-UF ₄
Enrichment	93.10 %	97 %/93 %	83.50 %	33.10 %	33.1 %	19.75 %	19.75 %	72 %/50 %/19.75 %	19.75 %/20 %/18 %	85 %/75 %/65 %	72 %/85 %/72 %	92 %	93 %
Cladding Material	–	SS	Re	Re	Re	TZM/SS	SS	Mo	ODS-MA754	W-Fe	ODS-MA754	Mo-Re	–
Matrix Material Heat Pipe Wall Material	– Haynes-230	SS	Re Mo-Re	Re Mo-Re	Re SS	Mo/SS FeCrAl (ODS)	Graphite Haynes-233	Mo Mo-Re	Mo W-Fe	– W-Fe	– ODS-MA754	Graphite Mo-Re	– Ni-based GH3535
Reflector Material Energy Conversion	BeO SE	Be SE	BeO AMTEC	BeO TEG	Zr ₃ Si ₂ TIC	Al ₂ O ₃ /BeO OBC	BeO SCO ₂ -CBC	BeO TEG	BeO SE & TEG	BeO OBC & closed-Rankine	Be/BeO SCO ₂ -CBC	Be He-Xe CBC	BeO SE/TEG
Reactivity Control	R	D	D	D	D	R&D	R& Sliding plate	R&D	R&D	R&D	R&D & Shim strips	R&D	R&D

Notes: Spectrum - F: Fast, E: Epithermal, T: Thermal; Heat Pipe Arrangement – S: Single-ended, D: Double-ended.

Notes: Energy Conversion - SE: Stirling Engine, OBC: Open-Brayton cycle, CBC: Closed-Brayton cycle; Reactivity Control - R: Rod, D: Drum.

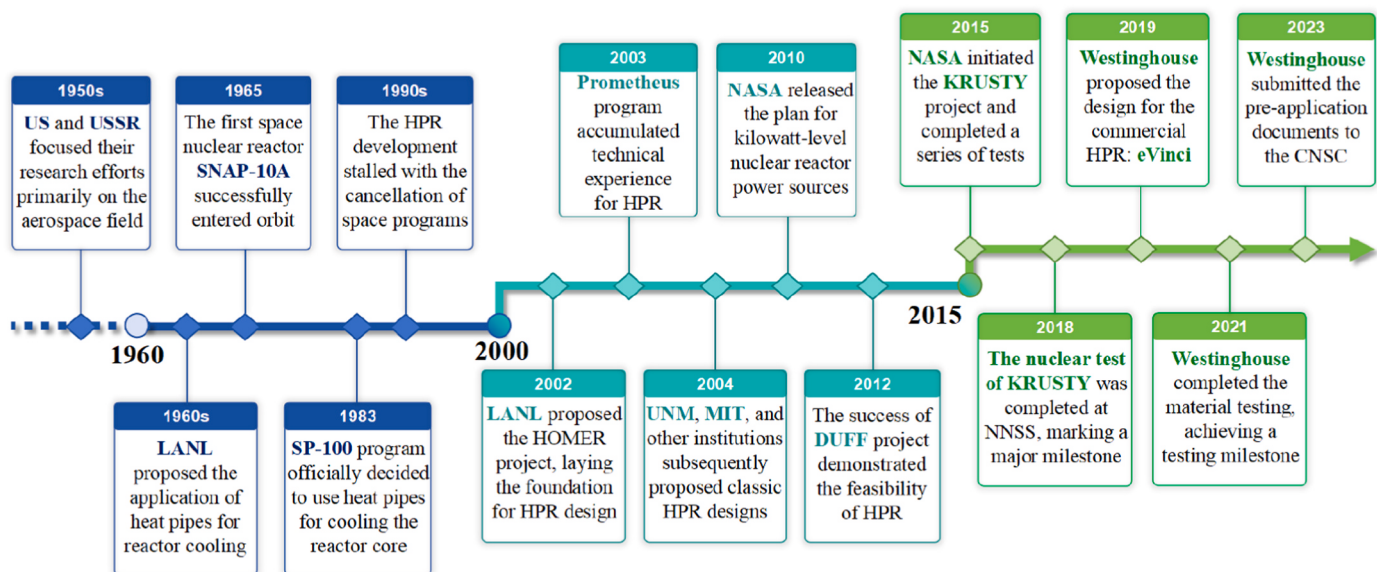


Fig. 4. The development history of HPR.

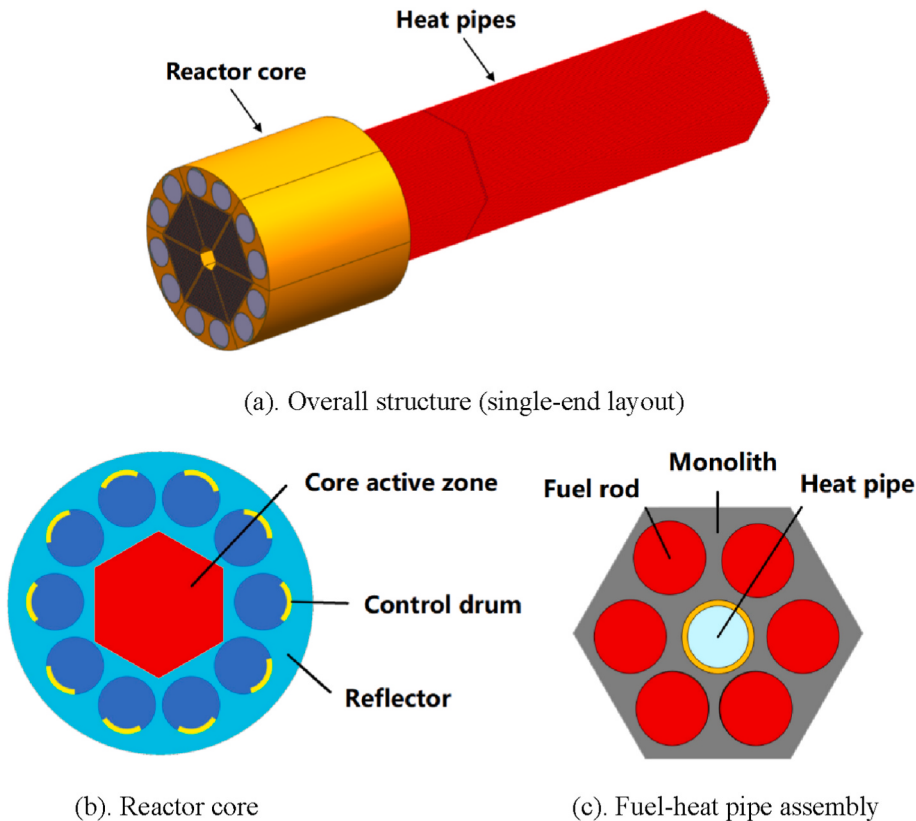


Fig. 5. A typical layout of an HPR [43].

sections: (i) evaporator, (ii) adiabatic, and (iii) condenser. Radially, (i) wall, (ii) wick, and (iii) vapor space.

HTHPs operate through the evaporation and subsequent condensation of the fully sealed working fluid [68], maintaining a continuous cycle. Heat is transferred as latent heat of vaporization, enabling an effective thermal conductivity exceeding that of metals by more than 100 times [69]. This self-driven process endows heat pipe-equipped systems with passive operational characteristics [70,71].

Alkali metals are the ideal working fluids for HTHPs in HPRs [72],

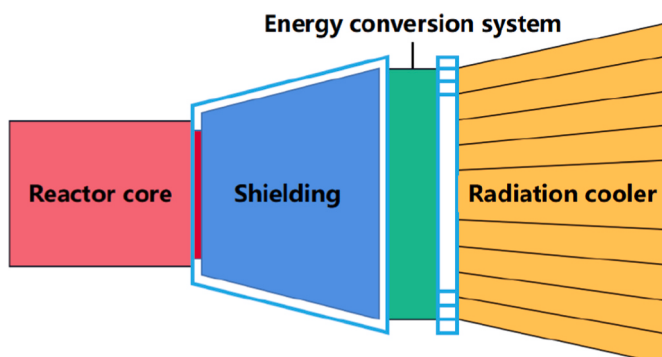
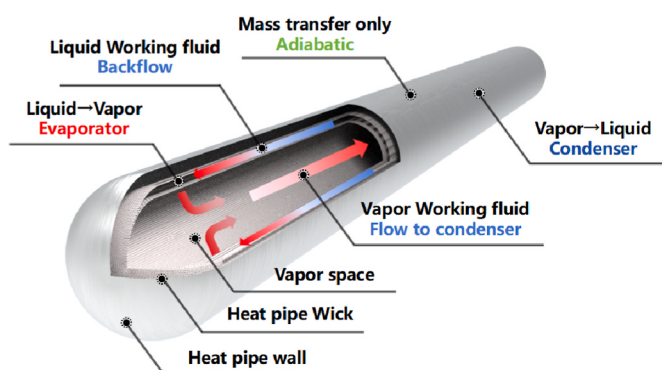
due to their high boiling points, low melting points, low saturated vapor pressures, high latent heats of vaporization, and suitable operating temperature ranges. This superiority is validated by their high Merit numbers [73]. The alkali metal working fluids available for use in HPRs are summarized in Table 3.

The consequences and risks of exposing alkali metals in HTHPs to air or water remain an unresolved gap in current research. Furthermore, the radiation resistance of these working fluids requires thorough evaluation, particularly for Li. Wang et al. [74] reported that Li in HTHPs

Table 2

Comparison of uranium-based nuclear fuels.

Fuel type	Uranium density (g/cm ³)	Melting point (K)	Thermal conductivity (W/m·K)	Advantages	Disadvantages	Ref.
UO ₂	9.7	~3080	2.8–3.3	- High chemical stability - Mature technology - Suitable for most reactors	- Poor thermal performance - Significant thermal expansion coefficient - Reduced uranium density	[54]
UN	13.5	~2903	21	- High uranium density - High thermal conductivity - Excellent thermal performance	- High chemical reactivity - Complex manufacturing process - High cost of N-15 production and processing	[55]
UC	13.2	~2798	27–35	- High uranium density - Excellent thermal conductivity - Good thermal performance	- Ultra chemical reactivity - Complex manufacturing process - Limited application, low technological maturity	[56]
UZrH	10.0	~2023	15–20	- Good thermal performance - Suitable for SMRs - Excellent negative feedback effect	- Low uranium density - Hydrogen content may cause embrittlement - Low melting point	[57]
UMo	15.8	~2890–3060	20–30	- Excellent uranium density - Good thermal conductivity - Excellent thermal performance - High melting point	- Complex manufacturing process - High uranium enrichment requirements - High sensitivity to alloy impurities	[58]
TRISO	~8.5 (depends on specific material layers)	~3273 (depends on specific material layers)	~15 (depends on specific material layers)	- High safety, multi-layer structure effectively prevents fission product release - Excellent high-temperature performance, up to 1800K - High mechanical strength - Non-proliferation	- Complex manufacturing process, high cost - Currently mainly used in high-temperature gas-cooled reactors - Relatively low volumetric density	[59]

**Fig. 6.** Schematic diagram of shadow shielding [43].**Fig. 7.** Typical working principle of a HTHP [67].**Table 3**

Comparison of alkali metals as HTHP working fluids for HPR.

Working fluid	Melting point (°C)	Boiling point (°C)	Operation temperature (°C)	Heat of vaporization (kJ/mol)
Lithium (Li)	180.54	1342	1000–1800	147.10
Sodium (Na)	97.72	883	600–1200	96.96
Potassium (K)	63.38	759	500–1000	77.40
Rubidium (Rb)	39.31	688	500–950	69.10
Cesium (Cs)	28.44	671	500–900	63.90

generates helium (He) under irradiation, releasing non-condensable gases that hinder the phase-change heat transfer.

3.2.2. Materials of HTHP wall

The HTHP wall is a crucial barrier that contains the working fluid and must possess several important characteristics to ensure reliability in reactor environments, including: 1) high irradiation resistance, 2) high strength and hardness, 3) good sealing, 4) nuclear stability, 5) chemical compatibility, 6) thermal expansion compatibility. Based on these requirements, several advanced high-performance alloys [44,45, 75–83] can be considered for wall materials, as shown in Table 4.

It is worth noting that Ni transforms into Co-60 under irradiation, producing intense secondary radiation [14], which complicates the relocation and redeployment of HPRs. Early designs considered nickel-free 30-series stainless steels; however, their high-temperature performance is subpar, with significant degradation occurring above 900 K [81]. ODS (Oxide Dispersion Strengthened steel), strengthened by the addition of dispersed metal oxides into FeCrAl matrix, offer a novel solution and are currently more widely adopted [14,47,49].

3.2.3. Configurations of HTHP wick

The wick generates the capillary force that drives the working fluid circulation, with its performance directly determining the heat transfer

Table 4

Comparison of wall materials suitable for HTHP.

Name	Main Components	Research Institutions	Temperature Limit/K	Advantages	Disadvantages	Ref.
Mo-Re alloy	Mo, Re	LANL	~2273 (Mo-41Re) ~1773(Mo-5Re)	- Exceptional high-temperature strength and creep resistance	- Extremely high cost (especially Re) - Low machinability - High-temperature oxidation issue	[44]
Hastelloy N	Ni, Mo, Cr, Fe	ORNL	~1123	- Excellent high-temperature corrosion and radiation resistance	- Very high cost - Low tolerance to long-term high-temperature irradiation and corrosion	[75]
KhN80MTY GH3535	Ni, Cr, Fe, Mo, Ti Ni, Cr, Mo	IAE SINAP	~1273 ~1023		- Very high cost - Limited availability - Almost no experimental data is available	[76] [77]
Incoloy 800H	Ni, Fe, Cr, Ti, Al	MIT	~1123	- Relatively good high-temperature corrosion and radiation resistance	- High cost - Susceptible to long-term high-temperature creep deformation	[78]
Haynes 230	Ni, Cr, W, Co, Mo	UIUC	~1423		- High cost - Low machinability - Prone to thermal fatigue	[79]
Inconel 617	Ni, Cr, Co, Mo, Al	CNRS	~1473		- High cost - The oxide layer may spall off under prolonged high-temperature	[80]
SS316	Fe(austenitic), Cr, Ni, Mo	ORNL	~1073	- Low cost and relatively mature manufacturing process	- Thermal resistance sharply decreases beyond 900K	[81]
SS304	Fe(austenitic), Cr, Ni	LANL	~1143	- Low Ni content enhances neutron economy and reduces the formation of Co-60		[45]
ODS Series	Fe(ferritic), Cr, Al, oxide particles	ORNL	~1373	- Both neutron economy and shielding requirements are better than 300-series SS	- Relatively complex manufacturing process - High brittleness under stress concentration	[82]

limit of the HTHP [72]. In the wick structure, capillary force and flow resistance exhibit a competitive relationship. As pore size increases, both capillary force and flow resistance decrease. Achieving an optimal balance between these factors is the primary focus of multi-objective optimization in wick design [83,84]. Table 5 summarizes the commonly used wick configurations in HTHPs. These configurations are often combined to overcome their respective limitations.

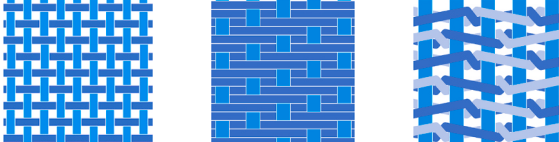
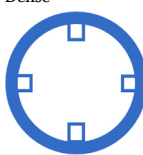
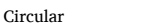
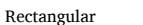
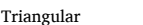
Moreover, metal foams are a promising option for HTHP wicks due to their high specific surface area and excellent wettability [85]. They are produced through a sintering process that directly forms an isotropic porous structure [86] (Fig. 8). Experimental studies [87–91] have demonstrated that metal foams outperform traditional wick

configurations in enhancing heat transfer and reducing thermal resistance. However, there is currently a lack of adequate theoretical models to describe the flow characteristic parameters within metal foams.

3.3. Integration of energy conversion system

The energy conversion methods in HPR systems are divided into dynamic and static types, based on whether mechanical moving parts are involved. For HPRs, four static conversion methods are currently available: Thermoelectric Generator (TEG), Thermionic Converter (TIC), Alkali Metal Thermal-to-Electric Converter (AMTEC), and Thermophotovoltaic (TPV). Additionally, four dynamic conversion methods

Table 5
ComHTHP.

Type	Configuration	Advantages	Disadvantages
Screen		- Easy to manufacture - High structural reliability	- Limited capillary carrying capacity
Arterial	Plain  Dense  Twill 	- High liquid supply efficiency - Greater capillary carrying capacity	- Low structural reliability - Prone to collapse
Grooved	Circular  Rectangular  Annular 		- Difficult to process - Reduces wall strength
	Circular  Rectangular  Triangular 		

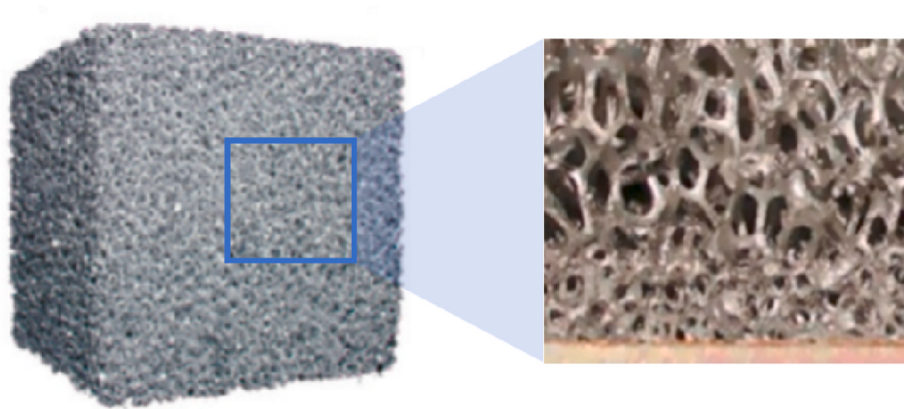


Fig. 8. Configuration of metal foam wick [85,86].

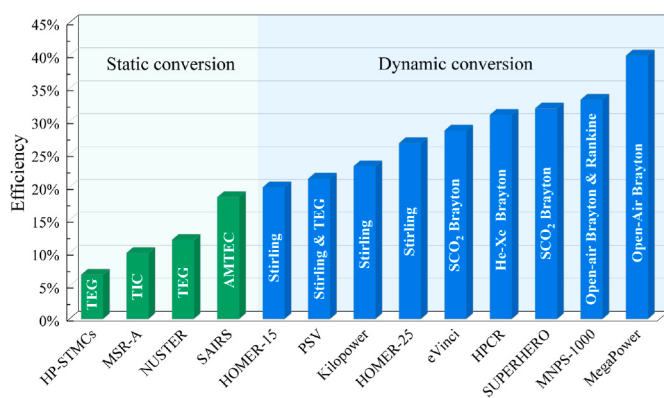


Fig. 9. Comparison of energy conversion systems used in current HPR designs.

are available: Magnetohydrodynamic (MHD), Stirling cycle, Brayton cycle, and Rankine cycle. Fig. 9 compares the energy conversion systems used in current designs. Compared to static methods, dynamic conversion methods generally provide higher efficiency but at the expense of reduced reliability, greater complexity, and increased noise levels. The comparison of these methods is summarized in Table 6.

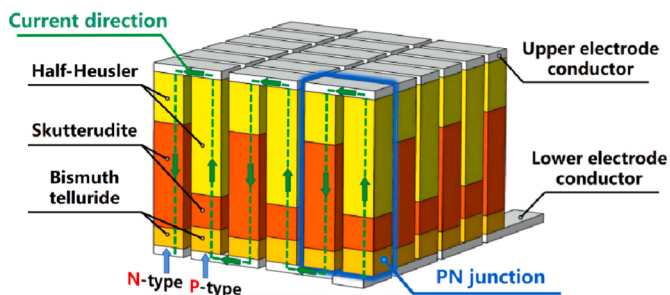


Fig. 10. Working principle of a three-stage STEG [103].

Table 6
Comparison of various energy conversion methods.

Type	Method	Efficiency	Advantages	Disadvantages	Ref.
Static conversion	TEG	~5% (single-stage) ~10% (two-stage) ~15% (three-stage)	- Simple and mature - Silent operation - High reliability - Integrable with the core	- High-temperature brittleness - Susceptible to single-point failure in series operation - Low efficiency - Extremely high operating temperature - Material challenges - Lower lifespan - Complex system - Severe electrical performance degradation - Corrosion issues - Limited by material performance - Waste heat dissipation issues	[92]
	TIC	10%-20%	- Silent operation - High reliability	- Material challenges	[93]
	AMTEC	20%-30%	- Silent operation - High efficiency at high temperatures - Lightweight	- Complex system - Severe electrical performance degradation	[94]
	TPV	~10%	- Silent operation - Low cost - Lightweight	- Limited by material performance - Waste heat dissipation issues	[95]
	MHD	50%-60%	- High potential efficiency - Power scalability	- Severe material corrosion - Under development	[96]
	Stirling cycle	20%-25%	- High efficiency - Small size and low noise - No phase change - Wide temperature difference applicability	- High shielding requirements - Vibrations caused by asymmetry	[97]
	Brayton cycle	30%-40%	- High efficiency - Simple structure - No phase change - Self-starting capability	- Additional ex-core system - Difficult to achieve theoretical efficiency - Slow thermal response	[98]
	Rankine cycle	25%-35%	- High efficiency - Well-established technology - Flexible working fluids	- More complex system - Requires phase change	[99]

3.3.1. Static conversion

3.3.1.1. Thermoelectric generator. TEG converts heat directly into electricity through thermoelectric effects [92]. To enhance the operating temperature and improve the conversion efficiency, Segmented-TEGs (STEGs) are increasingly employed in the design of HPRs (Fig. 10). These STEGs use different semiconductor materials in various regions based on temperature, allowing each material to operate within its optimal temperature range [100]. Studies show that the maximum efficiency of a two-stage STEG can reach up to 9.5 % [101], while the maximum efficiency of a three-stage STEG can exceed 14 % [102].

The high-temperature brittleness of TEGs is a major issue in their application to HPRs. HPRs typically require thousands of series-connected TEGs to generate sufficient power [103]. If the PN junction in a single TEG module fails, it could result in the failure of the entire branch, leading to a single-point failure in the energy conversion system. In addition, the relatively low efficiency of TEGs presents significant challenges for the design of waste heat removal systems, as they require the dissipation of a large amount of waste heat.

Currently, research in the TEG field primarily concentrates on developing novel high-performance thermoelectric materials. By adjusting dimensionality, controlling defects, and fine-tuning crystal structures, researchers aim to improve the thermoelectric figure of merit (ZT) [104,105]. Furthermore, given the complex, multidimensional, and nonlinear nature of TEG design, deep learning techniques have been effectively employed for optimization [106–108], offering substantial potential for advancing TEG applications in HPRs.

3.3.1.2. Thermionic converter. TIC utilizes the thermionic effect in metals (Fig. 11). Since electrons require sufficient energy to overcome the Fermi barrier, the emitter of a TIC can operate at temperatures above 1800 K [93]. This characteristic generally positions the TIC between the core and the HTHP rather than at the condenser section of HTHP.

The in-core TIC has already achieved success in the TOPAZ reactor [109] (Fig. 12). However, it is no longer the preferred choice for HPRs due to limited lifespan, as sustaining operation under ultra-high temperatures and intense radiation is very difficult. An alternative approach is to position the TIC at the condenser section of the HTHP. However, since most pure metal emitter materials operate at temperatures exceeding 1500 K [110], this strategy has long been constrained by the challenge of identifying non-pure metal emitter materials [111] that combine high-temperature stability (capable of sustained operation around 1000 K) with a sufficiently low work function (the minimum energy required for electron emission).

One promising solution is the coating method, which involves depositing a low work function material (such as metal oxides or diamond coatings) onto a high-performance emitter substrate [112]. This approach enables stable operation at temperatures of at least 1173 K [113], though its lifespan remains inadequate for meeting the operational demands of nuclear systems.

More recently, nano-intercalation techniques have emerged as an

innovative solution [114], with carbon nanotubes and graphitic carbon nanofibers standing out in particular. Their exceptional electrical conductivity and thermal stability enable emitter stability at temperatures as high as 1273 K [115]. This technological breakthrough is expected to be a key enabler for the future integration of TICs into HPRs.

3.3.1.3. Alkali metal thermal-to-electric converter. AMTEC achieves thermoelectric conversion by utilizing the properties of Beta Alumina Solid Electrolyte (BASE), which allows only alkali metal ions to pass through while blocking electrons and neutral atoms (Fig. 13).

AMTEC demonstrates relatively high efficiency among static conversion systems, with potential efficiencies reaching up to 30 % through optimized improvements [116], even surpassing certain dynamic conversion systems. The SAIRS design utilizes this conversion method (Fig. 14), achieving an efficiency of 18.5 % [31]. However, the lifespan of BASE in high-temperature environments is limited, and its electrical output characteristics will deteriorate rapidly in the later stages of its operational life.

Despite its potential, AMTEC still faces challenges related to chemical contamination and thermal degradation [117]. In particular, corrosive byproducts generated from the interaction between highly reactive alkali metals and structural materials can cause BASE blockage [118]. As a result, the highest reported laboratory efficiency remains below 20 %, significantly lower than its theoretical potential. Beyond the development of novel materials [119], a promising strategy for the future is the integration of AMTEC with TEG in a hybrid static power generation system [120]. This approach allows each technology to operate within its optimal temperature range, enhancing overall feasibility and performance.

3.3.1.4. Thermophotovoltaic. TPV directly converts thermal radiation into electrical energy [95]. Compared to photovoltaic power generation, TPV is driven by infrared radiation emitted from a high-temperature object, rather than by visible light [121].

Initially, TPV technology attracted significant interest in space power applications due to its lightweight and cost-effective nature [122], further benefiting from rapid advancements in photovoltaic cells. However, given the limitations of radiative cooling, the compatibility of TPV with HPRs is still under discussion. Challenges include its relatively low conversion efficiency, non-contact energy generation, and the difficulty in dissipating large amounts of residual heat. Therefore, utilizing TPV as a secondary energy conversion system might be a more viable option.

Additionally, due to the similar working principles of TPV (photon transfer) and TIC (electron transfer), recent research has explored integrating these technologies into a hybrid Thermionic-Photovoltaic (TIPV) system [123]. In this configuration, radiation energy not utilized by the TIC is further converted into electricity by the TPV, enabling direct secondary energy utilization, which has the potential to achieve a combined conversion efficiency of up to 30 % [124].

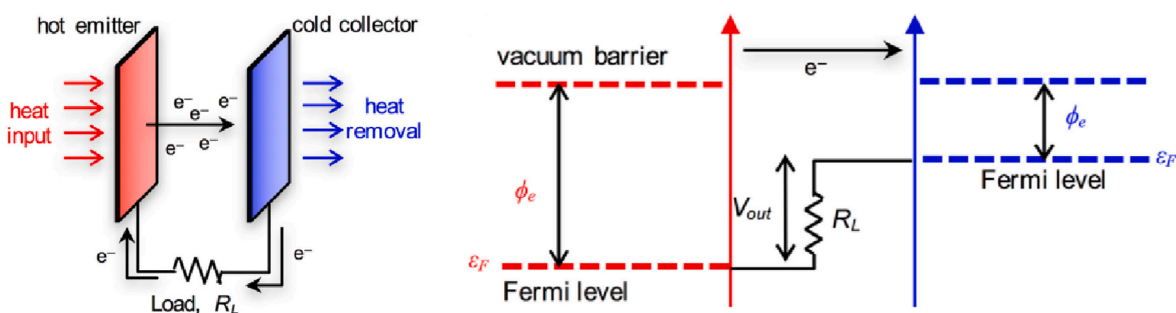


Fig. 11. Working principle of TIC [93].

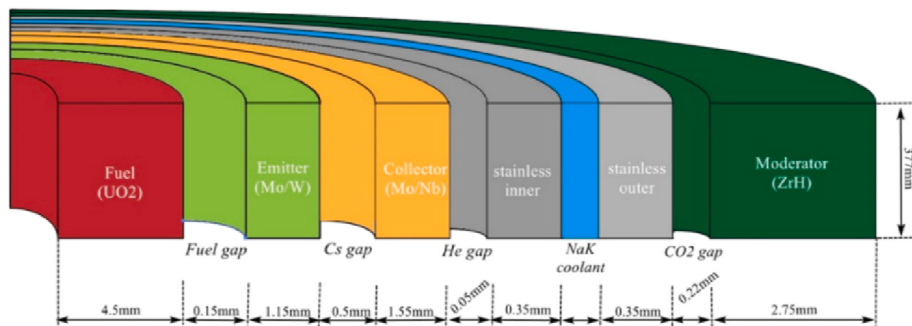


Fig. 12. Schematic of the thermionic converter in TOPAZ [109].

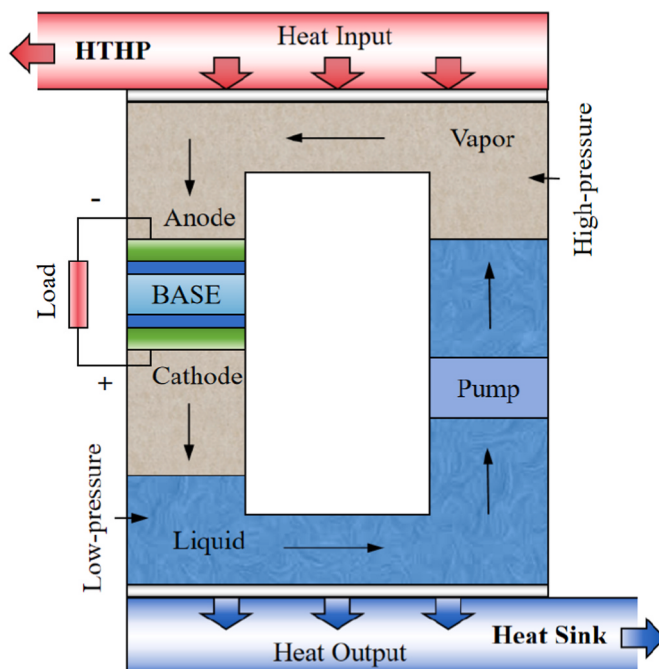


Fig. 13. Working principle of AMTEC.

3.3.2. Dynamic conversion

3.3.2.1. Magnetohydrodynamic. MHD generates an electromotive force by utilizing ionized fluids (gases, liquids, or plasmas) [125] that accumulate opposite charges as they are deflected while passing through a magnetic field region (Fig. 15). Although previous reviews [15,16] classify MHD as a static conversion method, it requires a precursor system to convert thermal energy into the kinetic energy of ionized fluids (Fig. 16). Based on this requirement, this review classifies MHD as a dynamic conversion method.

MHD generates electricity without the need for driving rotating components (such as generator rotors), resulting in minimal friction or mechanical losses and exceptionally high efficiency. NASA Marshall Space Flight Center combined MHD with gas-cooled reactors, achieving an efficiency of 55 % [126]. By incorporating processes such as

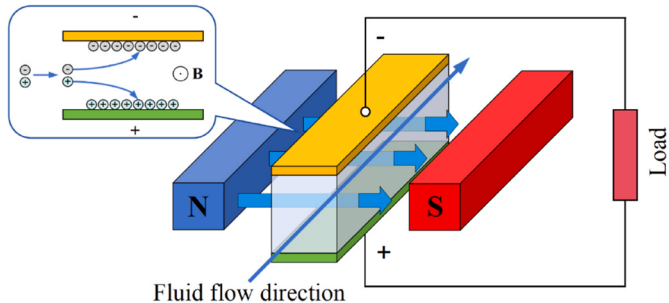


Fig. 15. Working principle of MHD.

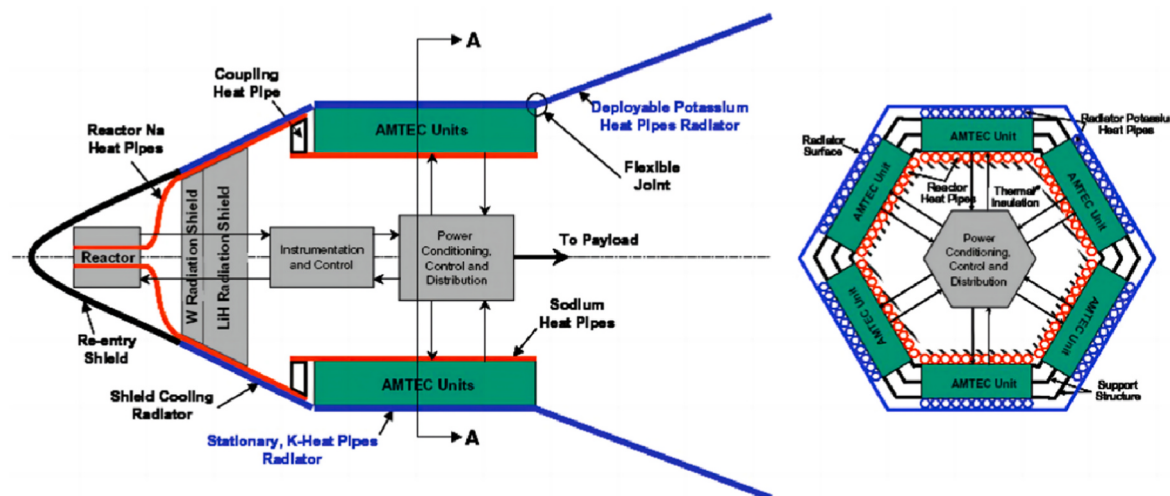


Fig. 14. Schematic of the AMTEC units in SAIRS [31].

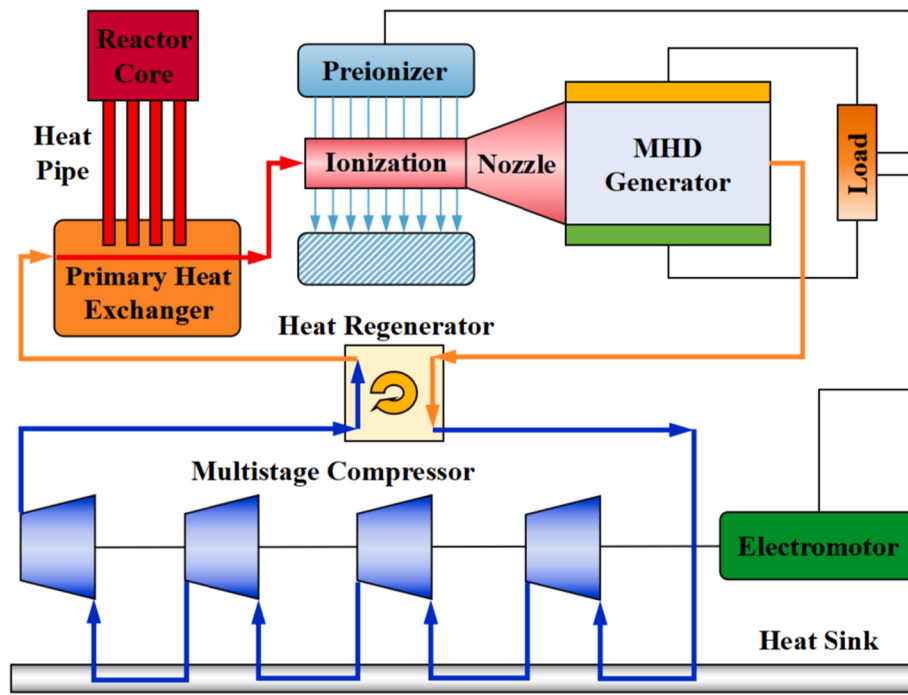


Fig. 16. Diagram of the MHD power generation system.

regeneration and reheating, MHD systems can reach efficiencies of up to 60 % [127]. Currently, although various MHD-based hybrid power generation systems have been proposed [125], the technology remains in its developmental stage and faces several challenges. The most critical issues include severe material corrosion and a limited operational lifespan [96]. Additionally, magnetic shielding and the flow instability of ionized fluids must be carefully addressed to enable future advancements [128].

3.3.2.2. Stirling cycle. The Stirling cycle is a simple and reliable external combustion, closed-loop piston power generation cycle [97]. In HPRs, the β -type Stirling engine is typically used (Fig. 17), consisting of two sets of coaxial pistons within the same cylinder, offering the highest spatial efficiency [129].

The Stirling engine combines the high reliability, long lifespan, and

lightweight characteristics of static conversion methods [130] with the high efficiency of dynamic conversion methods, making it an ideal choice for energy conversion. If the connecting rod is further eliminated, the system transitions into a Free-Piston Stirling Engine (FPSE), which further reduces mechanical wear while making the design more compact and quieter. Some studies suggest that optimizing the gas flow structure of the high-temperature heat exchanger in FPSE could even improve thermoelectric efficiency to 40.15 % [131].

The KRUSTY test [41] successfully demonstrated the feasibility of integrating Stirling technology with HPRs. To address the solid-solid assembly challenges, NASA Glenn Research Center adopted an integrated design [97], embedding the Stirling engine's heater into the heat pipe condenser (Fig. 18), significantly reducing interface thermal resistance. The primary challenges currently include vibrations caused by asymmetric operation of the multi-engines and the radiation

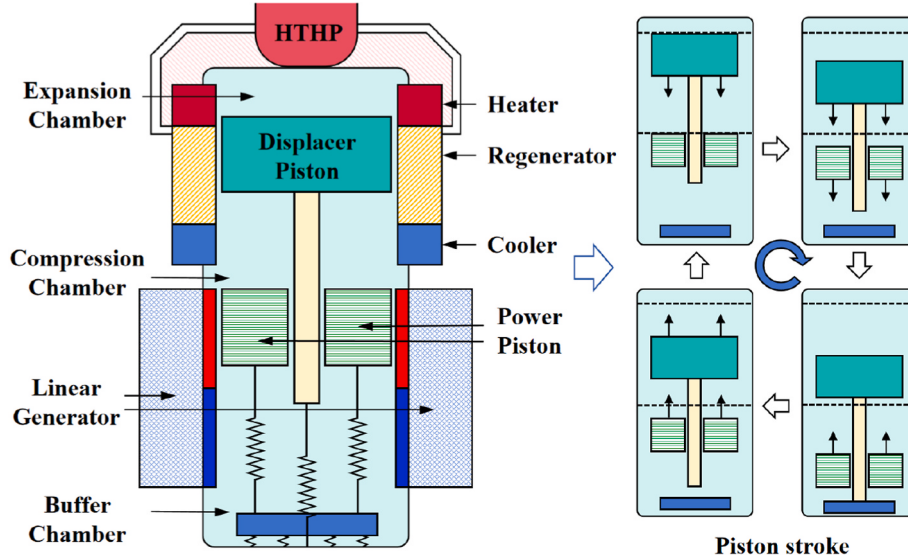


Fig. 17. Diagram of a β -configuration Stirling engine.

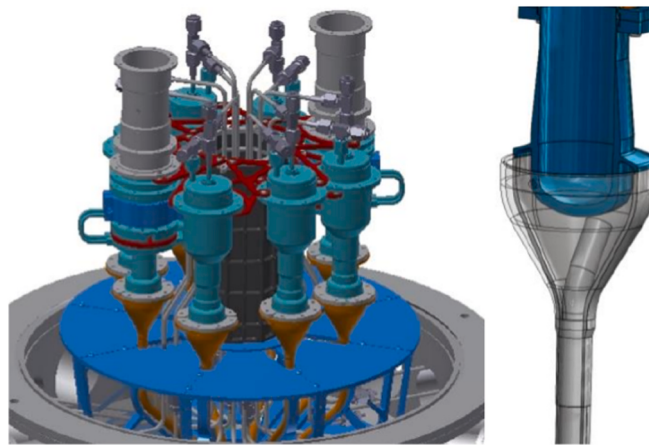


Fig. 18. Schematic of the eight Stirling engines in KRUSTY (Left) and the consolidated of Stirling engine with heat pipe (Right) [97].

shielding requirements for integrated systems.

3.3.2.3. Brayton cycle. The Brayton cycle offers a high level of technical maturity for nuclear applications [132]. Its non-phase change operation and self-starting capability make it a popular choice for HPR designs. A Brayton system can be equipped with a regenerator, reheater, or intermediate heat exchanger to improve efficiency, among which the regenerator-equipped configuration (Fig. 19) is considered the most cost-effective [53].

In terms of working fluids, open Brayton cycles using air as the working fluid have been widely adopted [98]. In recent years, closed Brayton cycle systems have demonstrated higher suitability for HPRs due to their smaller turbine volumes, lower probabilities of radioactive material leakage, and higher efficiency [133]. Among these, helium-based systems are relatively mature, with five out of nine closed Brayton cycle nuclear systems worldwide utilizing helium [134]. Helium-xenon mixture, which offer superior heat transfer capabilities, is also a viable option, albeit at significantly higher costs. Additionally, The Supercritical Carbon-dioxide (SCO_2) Brayton cycle is another promising choice. However, technical challenges, including the complexity of turbomachinery and material compatibility in high-temperature or near-critical regions, still require further

investigation [135].

3.3.2.4. Rankine cycle. The Rankine cycle uses a liquid working fluid, like water or liquid metal, and involves phase changes requiring evaporators and condensers [99]. This process complicates system design and reduces fault tolerance due to the need for precise pressure control. In practice, the Brayton and Rankine cycles are often combined into a "combined cycle" to enhance thermal efficiency [48]. Fig. 20 shows the thermal efficiency of these cycles at various turbine inlet temperatures.

The Rankine cycle can also be applied to the HPR residual heat removal system, primarily in the form of the organic Rankine cycle, which utilizes organic fluids to extract low-grade thermal energy for power generation [137]. This method demonstrates high compatibility with secondary power generation systems and radiative heat exchangers [32].

Although Rankine cycles exhibit high technological maturity [138], they are not well-suited for most HPR applications, resulting in limited research and analysis on their feasibility in this context.

4. Development and advances in HPR research

This section reviews the development and advances in HPR research, focusing on fundamental studies, technological improvements, and experimental validations. Key aspects such as theoretical modeling, innovative designs, and prototype testing are highlighted to provide a comprehensive understanding of the current research status.

4.1. Theory, experimentation, and progress in HTHP

4.1.1. Mathematical modeling

HTHPs significantly impact the thermal performance of HPRs, making them a key focus of theoretical research. However, the complexity of two-phase evaporative flow and heat transfer in HTHPs has prevented the development of a unified analytical model. Existing models, categorized by their level of simplification, include the Lumped Model (LM), Network Thermodynamics Model (NTM), Heat and Flow Model (HFM), Frozen Start-up Model (FSM), and Lattice-Boltzmann Model (LBM). Table 7 compares these models in terms of their accuracy, stability, robustness, speed, and resolution, highlighting their respective strengths and weaknesses.

4.1.1.1. Lumped model. The LM estimates the average HTHP

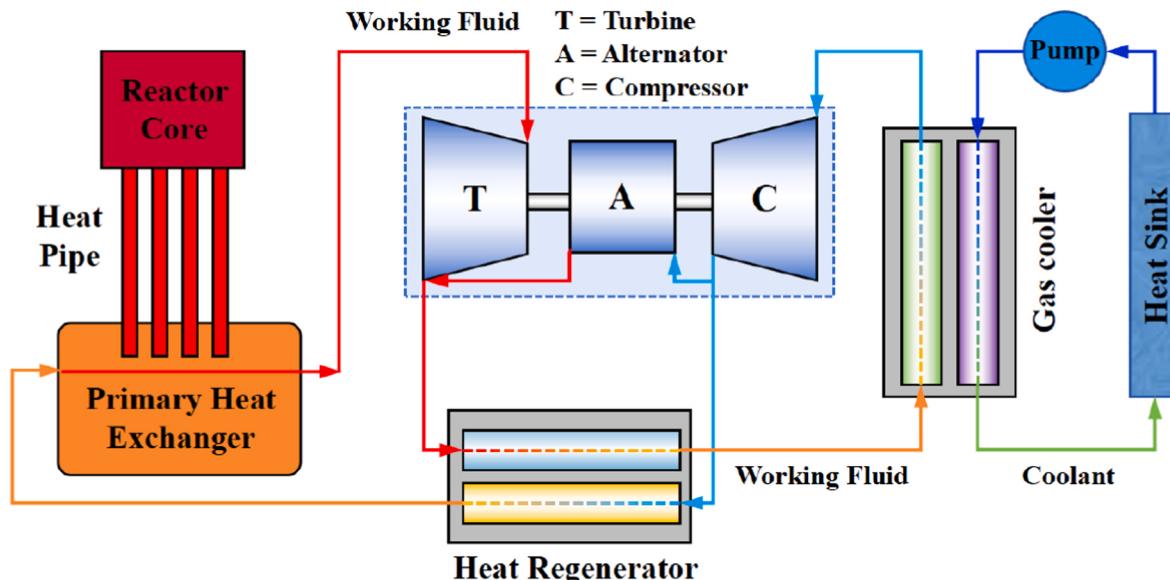


Fig. 19. Schematic of the coupling between the Brayton cycle and HPR.

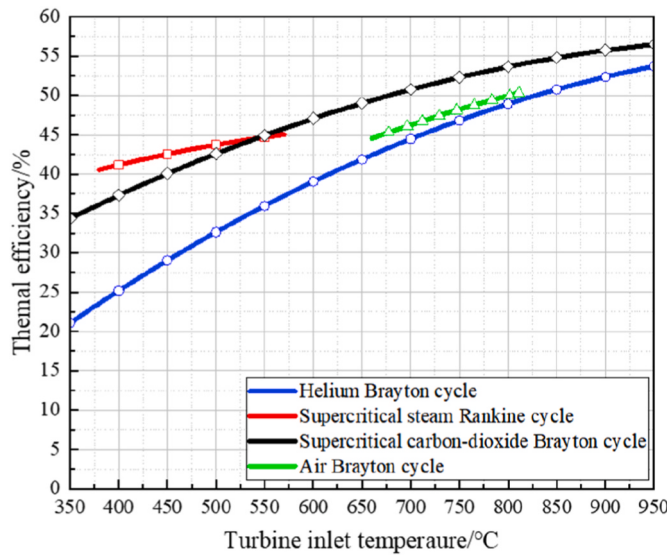


Fig. 20. Efficiency comparison of dynamic conversion methods with different cycles [136].

Table 7
Comparison of mathematical modeling of HTHP.

Model	Accuracy	Stability	Robustness	Speed	Resolution
LM	★★★★★	★★★★★	★★★★★	★★★★★	★★★★★
NTM	★★★★★	★★★★★	★★★★★	★★★★★	★★★★★
HFM	★★★★★	★★★★★	★★★★★	★★★★★	★★★★★
FSM	★★★★★	★★★★★	★★★★★	★★★★★	★★★★★
LBM	★★★★★	★★★★★	★★★★★	★★★★★	★★★★★

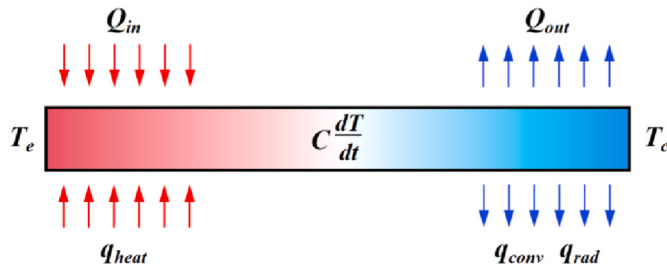


Fig. 21. Schematic of the LM

temperature using energy conservation principles (Fig. 21). While computationally efficient and suitable for preliminary HPR design [139, 140], its low resolution and strict Biot number constraints [68] limit its use.

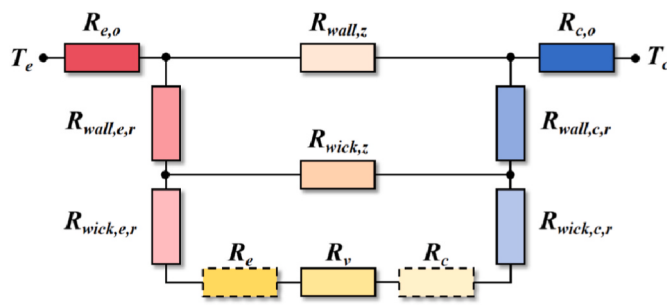


Fig. 22. Schematic of the NTM

4.1.1.2. Network thermodynamics model. The NTM, proposed by Zuo and Faghri [141], assumes that the working fluid flow has minimal impact on the transient temperature distribution due to slow liquid flow and low vapor density. Heat transfer processes are represented by thermal resistances [142], forming a network model similar to heat conduction in solids, also known as the thermal resistance network model. These thermal resistance generally includes (Fig. 22): (i) Evaporator outer thermal resistance $R_{e,o}$ and condenser outer thermal resistance $R_{c,o}$; (ii) Wall axial thermal resistance $R_{wall,z}$, evaporator wall radial thermal resistance $R_{wall,e,r}$, and condenser wall radial thermal resistance $R_{wall,c,r}$; (iii) Wick axial thermal resistance $R_{wick,z}$, evaporator wick radial thermal resistance $R_{wick,e,r}$, and condenser wick radial thermal resistance $R_{wick,c,r}$; and (iv) Vapor axial thermal resistance R_v . Additionally, evaporation phase change resistance R_e and condensation phase change resistance R_c can also be considered, but their magnitudes are generally negligible.

The NTM provides higher resolution than the LM, faster computation than the HFM, especially for steady-state calculations, with a relative deviation typically within 5 % [141]. Over 80 % of existing HPR numerical simulations employ the NTM.

4.1.1.3. Heat and flow model. The HFM aims to establish the relationships between the temperatures of different heat pipe regions and the boundary conditions [68,142], reflecting the thermodynamic properties and thermal response of the wall, wick, and vapor space. It is divided into the wall, wick, vapor space, and Liquid-Vapor Interface (LVI) models (Fig. 23).

- (1) Wall: The heat conduction equation is used for the wall, with heat flux boundary at the evaporator and convection boundary at the condenser.
- (2) Wick: The small pore scale (10^{-4} m) makes modeling the complete structure challenging. Two simplification methods are available: (i) neglecting flow within the wick and treating it as a solid [143] with equivalent properties [144], which doesn't capture flow-induced phenomena such as dry-out; (ii) using a porous media model to describe flow within the wick, which involves solving the laminar, incompressible Navier-Stokes equations [145], but is computationally intensive.
- (3) Liquid annulus: A liquid annulus between the wall and wick is commonly treated as part of the wick with porosity of 1 [146].
- (4) Vapor space: The varying physical properties of alkali metals make higher-order vapor equations challenging to converge, particularly when coupled with the LVI. Commonly used vapor flow models include quasi-steady one-dimensional compressible [147,148], transient one-dimensional compressible [149,150], transient two-dimensional compressible [151], and non-condensable gas [152,153]. These studies, supported by experimental [154–156] and theoretical [157,158] evidence, typically assume laminar vapor flow.
- (5) LVI: The LVI coupling conserves mass, momentum, and energy. The mass exchange rate is determined using either the molecular dynamics equation [159] or the Lee phase-change equation [160], both of which require pre-adjustment factors to suit different scenarios. The Lee equation uses a semi-empirical coefficient [161], while the molecular dynamics equation employs the phase-change adjustment coefficient (a_{cc}). The a_{cc} depends on factors such as fluid temperature, flow velocity, and the position and shape of the LVI, making a fixed value unsuitable for all cases [162]. The primary challenge lies in the absence of a definitive theory for calculating a_{cc} , with only approximate segmented values available [163]. Momentum coupling describes the interactions among capillary forces, liquid, and vapor [164–167], while energy coupling is primarily governed by the mass exchange rate and the latent heat of vaporization.

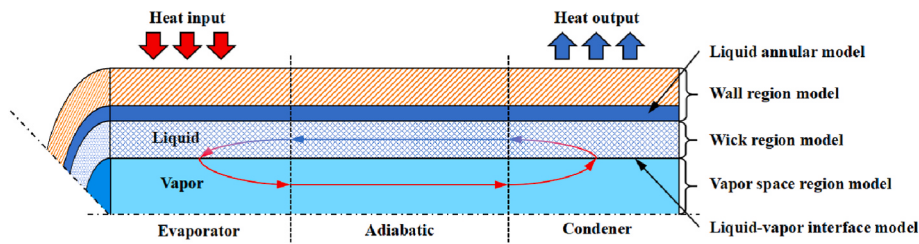


Fig. 23. Main heat pipe modeling regions.

4.1.1.4. Frozen start-up model. In HTHPs, alkali metal working fluids are solid at room temperature, necessitating a frozen start-up process. Experiments [168,169] reveal that this process is gradual, with each point inside the HTHP quickly reaching operating temperature, rather than a uniform system-wide temperature rise. The FSM encompasses heat and mass transfer mechanisms during different start-up stages [170]. It integrates various models to describe the heat transfer characteristics of the vapor-liquid-solid phases [171–174] as the HTHP transitions from room temperature to steady-state (Fig. 24).

Compared to the HFM, the FSM assumes a moving "front" within the wick and vapor regions, identifying the front of melting [176–178] and vapor flow regime transitions [179–182]. This enables calculations to begin from a fully frozen HTHP state but significantly increases computational demands and reduces stability. The challenge arises from the drastic changes in alkali metal properties between room temperature and 1000 K, where saturation pressure shifts by 5–6 orders of magnitude [68]. To maintain stability, more relaxed conditions and smaller time

steps are necessary.

4.1.1.5. Lattice-Boltzmann method. The LBM models the macroscopic behavior of fluids through particle distribution functions, making it particularly suitable for investigating multiscale problems in HTHPs. LBM excels in mesoscopic scale problems, handling complex geometries, and simulating multiphase and multicomponent flows, including phase changes. Its scalability and ability to model porous materials, which are challenging for traditional Computational Fluid Dynamics (CFD), make it particularly suitable for HTHP applications [183]. Notably, LBM can describe flow and heat transfer across all phases in HTHP without requiring additional closure models.

The LBM method has already seen some applications in heat pipe. Grissa et al. [184,185] used LBM to simulate heat pipes under an axisymmetric coordinate system, achieving results that matched very well with reference values. Liu et al. [186] applied LBM to study seepage in porous media and found discrepancies between simulation results and the Carman-Kozeny equation for permeability estimation.

4.1.2. Thermal performance testing

Numerous metrics are used to evaluate the performance of HPRs, with current research primarily focusing on the isothermality [187–189], thermal resistance [190,191], and heat transfer limits [192–194] of HTHPs in HPRs. Factors considered critical to the thermal performance of HTHPs include the working fluid, filling ratio, geometry, wick configuration, and materials. Table 8 summarizes studies on the thermal performance of HTHPs suitable for HPRs.

The studies summarized in Table 8 provide important design references for the application of HTHPs in HPRs, including working fluid selection [188,192], material selection [14,189], and optimal filling ratios [190,194]. Furthermore, these studies have identified novel phenomena related to three critical limits: the capillary limit [187], boiling limit [191,193,194], and entrainment limit [192]. Additionally, the ultra-long-term testing of Na compatibility with MA-ODS 754 [189] represents a milestone in HTHP research, demonstrating the superiority of MA-ODS 754 for HPR systems and establishing it as the current material of choice in reactor designs [47,49]. However, the current limitation lies in the lack of research focusing on different wick configurations, as most studies have exclusively employed screen wicks.

The inclination angle also affects the characteristics of HTHPs, as HPRs do not always operate at a horizontal orientation. Inclination primarily affects the return flow of liquid in HTHPs, with minimal impact on the vapor phase or liquid-vapor interactions [192]. A positive angle enhances capillary force with gravity, aiding HTHP performance, while a negative angle hinders it. Although inclination is irrelevant in space, it is critical for land and sea applications to evaluate the "worst-case scenario" for HPR. Table 9 summarizes key studies on HTHP inclination angles relevant to HPR.

Due to the high operating temperature, extremely low saturated vapor pressure, and stringent sealing requirements of alkali metals in HTHPs, current testing is limited by measurement techniques. Most evaluations rely solely on the temperature of the outer wall as an indicator, neglecting critical parameters such as fluid velocity, pressure, and the shape of the LVI. The success of X-ray imaging technology [194] and

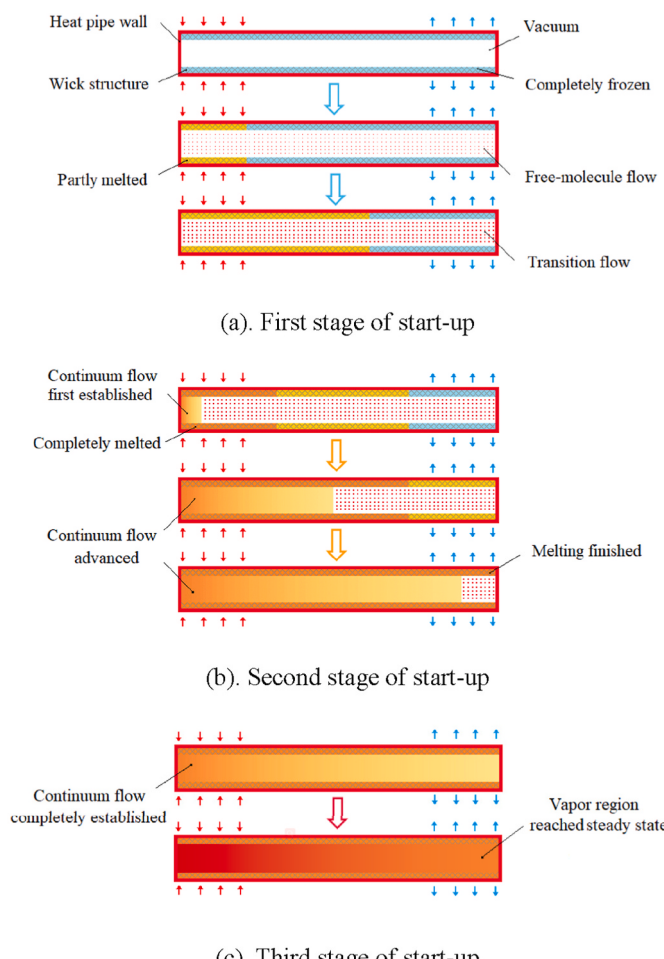


Fig. 24. Schematic of the frozen start-up process of HTHP [175].

Table 8

Studies on HTHP thermal performance and key findings.

Ref.	Working Fluid	Filling	Geometry/mm	Wick	Materials	Working condition	Key findings
Chen et al. [187]	Cs	48g	Φ32 × 600	Screen (400 &100-mesh)	In600	772.5–940.9–1300.9W	- Modulated heating could avoid capillary limit, raising operating temperature from 413 °C to 500 °C
Dussinger et al. [188]	Cs/K	–	Φ38.1 × 610	Screen	CP Grade 2 Ti	48h-test, 580–720K	- Ti/K HTHP significantly outperform Ti/Cs HTHP above 740K, whereas the performance is reversed between 550 K and 740 K
Swartz er et al. [14]	Na	–	Φ22.6 × 1200	Screen	FeCrAl	2850h-test, 800 °C	- No measurable change in HTHP performance was observed through the duration of test
Reid et al. [189]	Na	–	Φ19.1 × 457	Screen (100-mesh)	MA-ODS 754/ MA-ODS 956	>5500h-test, 1223K	- MA-ODS 956 failed after 140 h, while the MA-ODS 754 capsule remained operational for over 5500 h
Manoj et al. [190]	Na	40 %	Φ10 × 1000	Screen (2 × 60 &150-mesh)	SS316	1600W, forced helium cooling	- Na/SS HTHP perform better at a filling ratio of 40 %
Lee et al. [191]	Na	65.7g	Φ25.4 × 1000	Screen (2 × 60-mesh)	SS316	491–1205W, air natural cooling	- Na/SS HTHP continue to operate even when subcooled boiling occurs
Wang et al. [192]	K	20g/100g	Φ30 × 800	Screen (300-mesh)	SS316	800W, air natural/water forced cooling	- The entrainment limit can also lead to dry-out in addition to the capillary limit
Zhang et al. [193]	NaK	70g	Φ25 × 800	–	Inconel 600	800–1400W, water forced cooling	- Under forced convection cooling conditions, geyser boiling can occur in the condenser before a continuous flow is established
Huang et al. [194]	Na	67 %/102 %/172 %	Φ25.4 × 1016	Screen	SS304	500–3800W, air forced cooling	- X-ray imaging was used for the first time to observe two-phase flow and boiling behavior in HTHPs, revealing the occurrence of geyser boiling phenomena

Table 9

Studies on HTHP inclination angle and key findings.

Ref.	Working Fluid	Filling	Geometry/mm	Wick	Materials	Working condition	Key findings
Chen et al. [195]	Cs	48g	Φ32 × 600	Screen (400 &100-mesh)	In600	317.2–1416.2W, 0°–80°	- HTHP achieves optimal inclination at 68° rather than 45°
Tian et al. [196]	Na	158g/208g	Φ30 × 2000	Screen(300-mesh)	Haynes 233	1.21–5.85 kW, 0°–90°	- At 80°, the isothermal performance at the end of the condenser significantly deteriorates
Ma et al. [197]	Na	20 %	Φ20 × 1000	Screen (400 &100-mesh)	SS316	8 groups of 1.05–1.29 kW, –15°–45°	- The Chi model is suitable for evaluating the horizontal capillary limit but proves inadequate for inclined conditions
Guo et al. [198]	NaK	70g	Φ25 × 1000	None	In600	725 °C, 0°–80°	- The periods and amplitudes of heat transfer oscillations effected by inclination angle is nonlinear
Tian et al. [168]	K	20g/100g	Φ35 × 800	Screen(300-mesh)	SS31608	9 groups of 200–4000W, –15°–90°	- Angle increases from 0 to 50°, the starting time is greatly reduced, and the reduction is not obvious from 50° to 80°
Wang et al. [199]	K	15g	Φ30 × 800	Screen (300-mesh)	SS31608	360–600W, –15°–90°	- At a 30° inclination angle, a 100 % K filling ratio achieves optimal heat transfer
Ma et al. [200]	Na	20 %/30 %/40 %	Φ32 × 400	Screen (100/4400-mesh)	SS304	600–900W, 15°–45°	- The gravitational effect under negative inclination angles may lead to startup failure
							- Using intrusive measurements, the influence of multiple factors on the nucleation superheat of geyser boiling was investigated

advancements in intrusive measurement techniques [200] offer new possibilities for future measurements.

4.1.3. Nanostructure modification

Nanotechnology holds great promise for improving heat transfer in HTHPs without modifying design parameters. Due to their size being much smaller than the microporous structure of the wick, nanoparticles rarely cause clogging. When introduced, nanoparticles adhere to the wick structure [201], altering the capillary radius, forming a hydrophilic surface [202,203], enhancing surface roughness and wettability [204–207], and improving capillary performance [208–211]. This enhances working fluid circulation, delays the heat transfer limit, and optimizes heat pipe performance.

For nanofluids as working fluids, Arya et al. [212] reported a 40 % enhancement in heat transfer performance using carbon nanotube nanofluids with a screen mesh wick. Tsai et al. [213] demonstrated significant reductions in evaporation thermal resistance with gold nanofluids. Wang et al. [214] observed up to 50 % reduction in total thermal resistance and a 40 % improvement in heat transfer efficiency with copper nanoparticle nanofluids. Similarly, Moraveji et al. [215]

found that Al₂O₃ nanofluids reduced thermal resistance and enhanced isothermality, thereby improving heat transfer efficiency. Zhou et al. [216] identified that a 0.05 wt% concentration of graphene nanofluids achieved optimal start-up performance.

In surface modification applications, Gupta et al. [217] used physical vapor deposition to coat wick surfaces with TiO₂ nanoparticles, reducing thermal resistance by 12.1 % and increasing thermal efficiency by 11.9 %. Tharayil et al. [218] achieved a 22.6 % reduction in thermal resistance and an 86 % increase in the evaporator heat transfer coefficient by coating copper nanoparticles on mesh wicks. Jyothi et al. [219] employed a sol-gel method to create a uniform TiO₂ coating on copper mesh wicks, enhancing wettability and heat transfer efficiency by 12 %.

Research on nanomodification has similarly been limited to the selection of nanofluids, neglecting the impact of modified wick configurations. Future studies should expand to include wick parameters, particularly the effects of increased mesh intersection points at high mesh counts on the macroscopic heat transfer characteristics of nanofluids.

4.2. Innovative design concepts in HPR

Table 1 lists the major HPR designs, most of which follow the principles established by the HOMER series. This section mainly introduces the concept design with "characteristic" in recent years, which have higher power outputs and innovative design concepts, resulting in different solutions than traditional designs.

4.2.1. First commercial solution: eVinci

The eVinci, developed by Westinghouse, is currently the most promising candidate for the first commercial HPR demonstration [220], which employs LEU with an enrichment level of 19.75 %. Its design integrates several innovative features (Fig. 25), including TRISO fuel with stainless-steel-coated UN/UO₂, metal hydride moderation tailored for an epithermal spectrum and LEU, and a Na-HTHP with a FeCrAl (ODS) outer wall. Designed for remote applications, eVinci aims to deliver a stable energy supply with an operational lifespan of up to 10 years.

4.2.2. Underwater energy supply: NUSTER

The NUSTER (NUclear Silent Thermal-Electrical Reactor) is designed for heavy Unmanned Underwater Vehicles (UUVs), providing 100 kW_e [46]. To ensure silent operation, it uses a fully static energy conversion system with over 8000 TEGs. These TEGs have their hot ends connected to Na-HTHPs and cold ends to cold plates, forming a "sandwich-like" structure. For better integration of the energy system, the reactor core adopts a rectangular design instead of the traditional hexagonal shape (Fig. 26).

NUSTER employs three-stage STEGs constructed with half-Heusler, skutterudite, and bismuth telluride materials. Theoretical efficiency reaches 15.5 % [221], with an average efficiency of 14.4 % [103], even after considering temperature distribution non-uniformity. Residual heat is dissipated into seawater, and in emergencies, seawater backflow ensures long-term cooling for safety.

4.2.3. Dual-mode mobile power vehicle: PSV

Power Supply Vehicle (PSV) is designed for land-based deployment [47]. They feature dual-mode power generation: TEG units for static thermoelectric conversion on one end and six opposed Stirling engines for dynamic conversion on the other. A hybrid energy storage system, combining power batteries and supercapacitors, stores generated electricity (Fig. 27). This dual-mode design enables adjustable static-to-dynamic power ratios across various ranges, offering key advantages [222]: (1) ultra-silent, stealthy operation in low-power mode; (2) high efficiency and output in high-power mode; (3) compact and rational layout; and (4) self-starting and self-regulating capabilities for simplified control.

The system produces 230 kW of power, and can supply up to 400 kW with batteries and supercapacitors, ensuring adequate energy for variable speed movement scenario.

4.2.4. Modular core designs: MNPS and SUPERHERO

4.2.4.1. MNPS. The Mobile Nuclear Power System (MNPS) is a large-scale HPR [48], delivering 1000 kW_e. Unlike traditional monolithic core designs, the MNPS features a modular core composed of 36 fuel

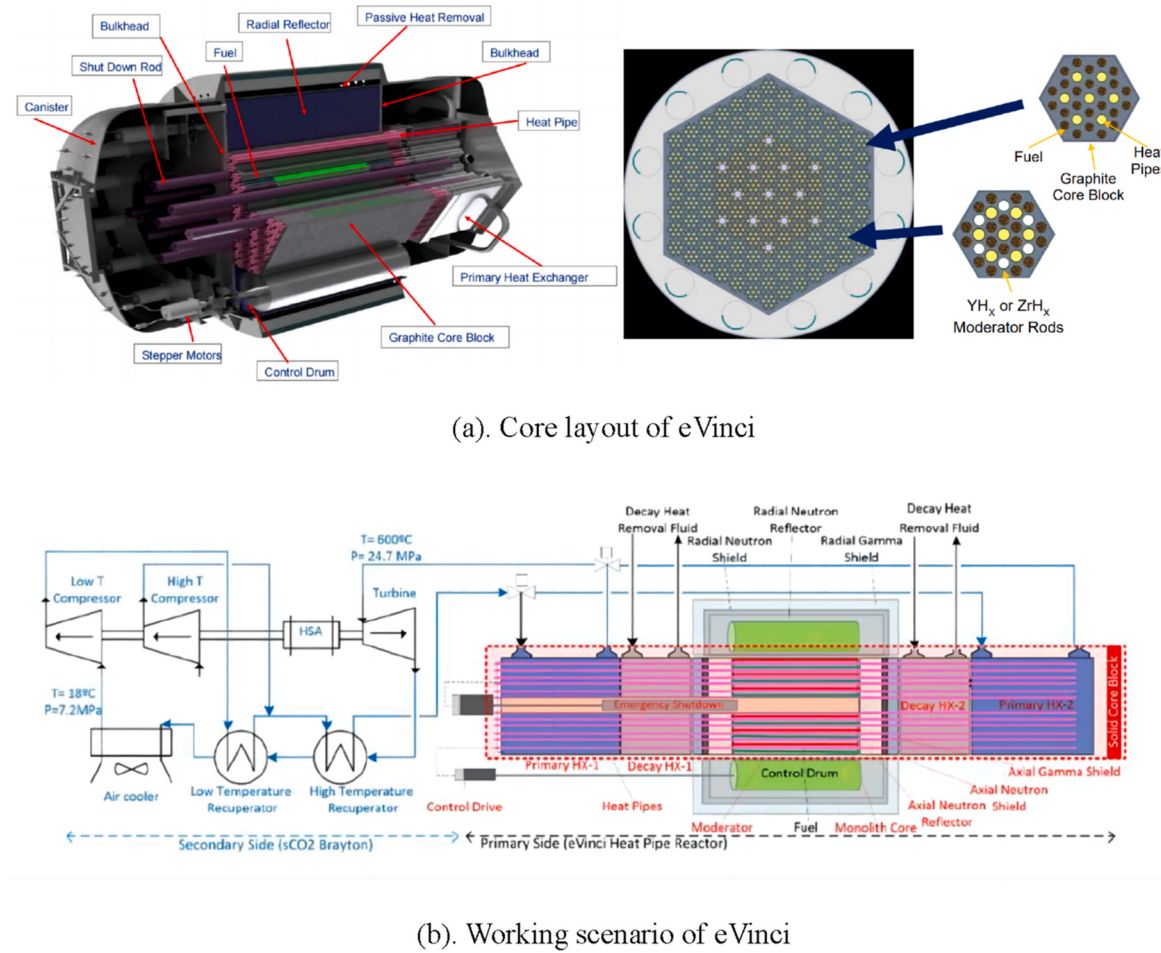
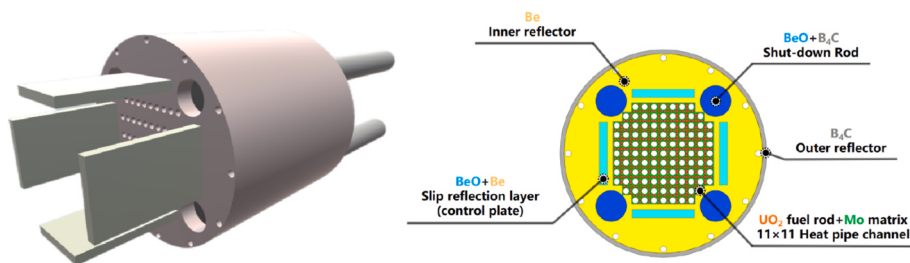
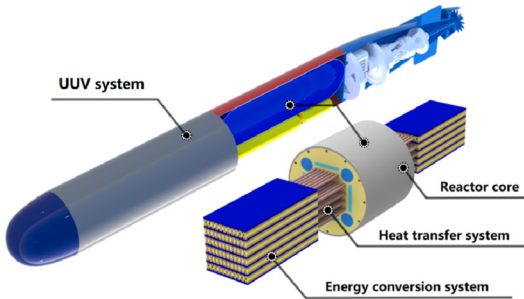


Fig. 25. Schematic design of eVinci [14].



(a). Core layout of NUSTER

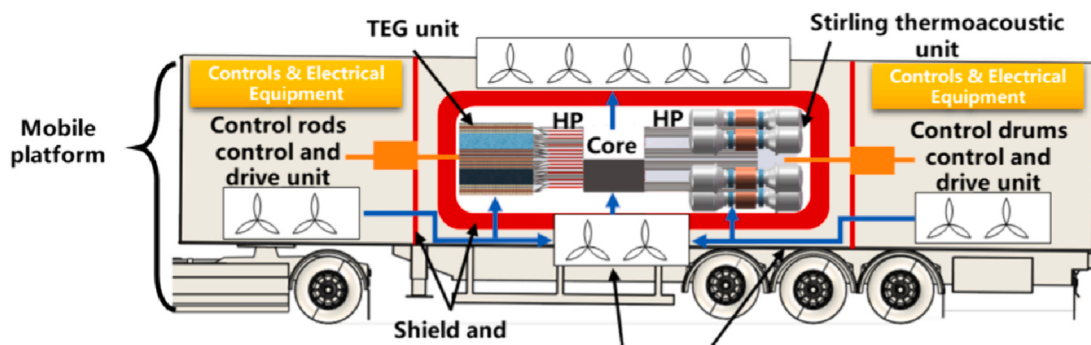


(b). Working scenario of NUSTER

Fig. 26. Schematic design of NUSTER [103].



(a). Core layout of PSV



(b). Working scenario of PSV

Fig. 27. Schematic design of PSV [47].

assemblies (Fig. 28). Each fuel assembly consists of W-Fe cladding with dispersed UN fuel and incorporates six Li-HTHP channels. This design mitigates stress concentration caused by severe thermal expansion in the solid core.

In terms of energy conversion, the MNPS employs a combined cycle

consisting of an open Brayton cycle and a closed Rankine cycle, achieving a system efficiency of 33.3 %.

4.2.4.2. SUPERHERO. The SUPERHERO (SUPERcritical carbon dioxide cycle-HEat pipe ReactOr power system) is a fast-spectrum HPR equipped

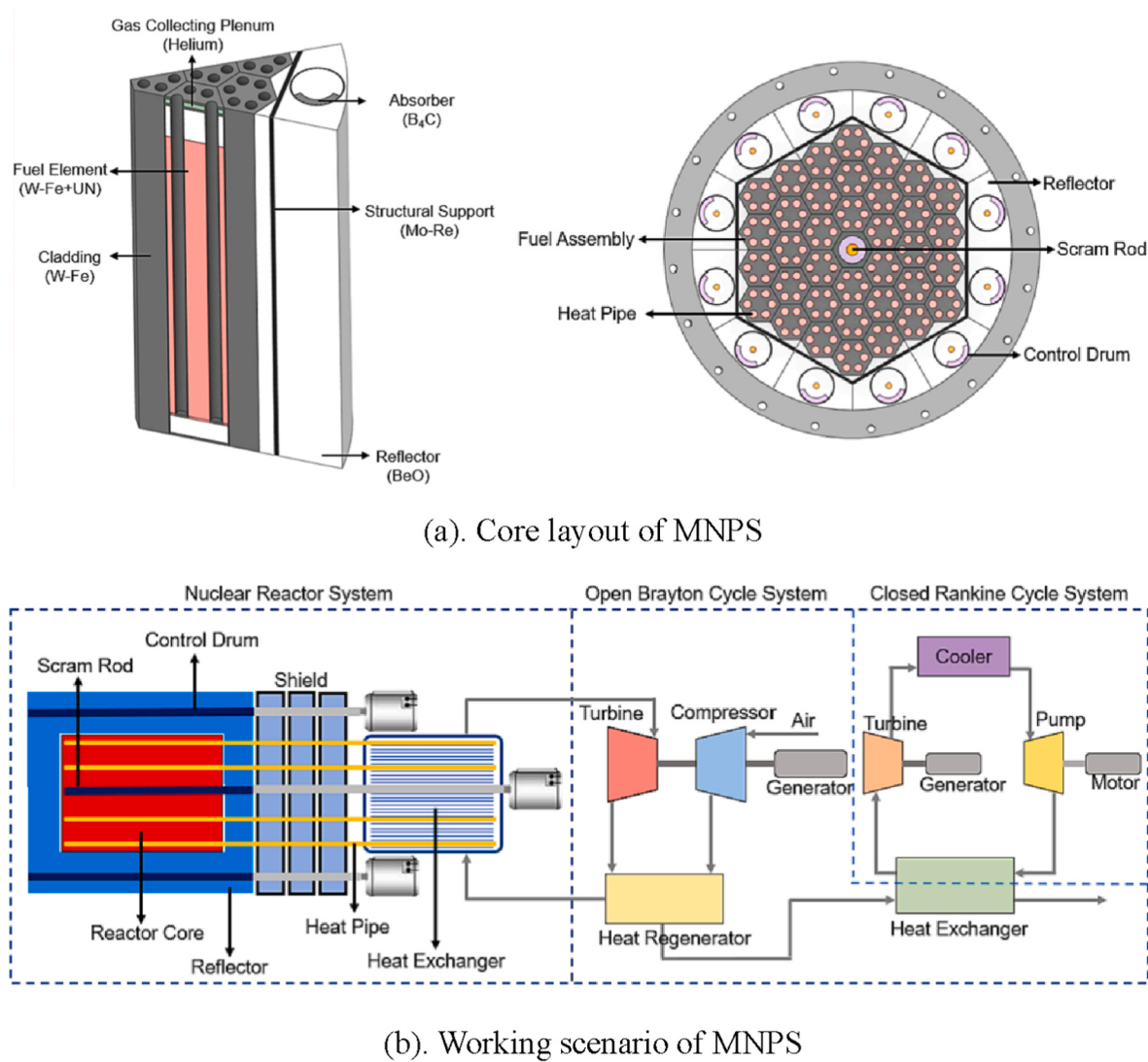


Fig. 28. Schematic design of MNPS [48].

with K-HTHPs and utilizing an SCO_2 Brayton cycle, capable of producing 1000 kWe [49]. SUPERHERO surpasses the MNPS in modular core design by completely abandoning core-perforated designs. Instead, the entire core is assembled from 390 HTHP modules (Fig. 29), each consisting of a hexagonal fuel ring fitted around the evaporator of the HTHP. A reflector layer is placed between the fuel ring and the HTHP, with ODS-MA754 used as cladding to securely encapsulate the fuel and provide structural strength. This system features a simple closed Brayton cycle. By using SCO_2 as the working fluid, SUPERHERO achieves an efficiency comparable to MNPS despite operating at a lower temperature.

4.3. Construction and testing of HPR prototypes

4.3.1. HPR-Stirling prototype

The KRUSTY experiment comprehensively demonstrated the feasibility, performance, and safety of the HPR-Stirling coupled system [223]. The test utilized specialized UMo fuel (92 % uranium, enriched to 93.1 %, and 8 % molybdenum) with only eight Na-HTHPs transferring heat from the core to four opposed Stirling engines (Fig. 30). The reactor was placed in a vacuum environment, and its reactivity was controlled by adjusting the reflector insertion depth using a lifting mechanism. This experiment marked the first full-system nuclear loading test of an HPR.

KRUSTY provided a comprehensive set of analyses [224], design

[225], and test reports [226], establishing a foundational database for reactor startup, power ramp-up, load following, steady-state operation, shutdown, and accident conditions. Current studies widely utilize experimental data obtained from KRUSTY for validation purposes.

4.3.2. HPR-TEG prototype

Since 2019, Xi'an Jiaotong University (XJTU) has been testing HPR-TEG prototypes to explore the feasibility of integrating HPR technology with TEG and Stirling systems. Key prototypes include HPTEG-1.0 [227], which demonstrated silent energy conversion at moderate power levels (<100 kW), and HPTEG-2.0 [222], which focused on high-power systems (<1 MW) combining TEG and Stirling technologies. Both prototypes are non-nuclear and use electric heating.

HPTEG-1.0 employs seven K-HTHPs for heat transfer, supported by two copper-based structures (Fig. 31). Power is generated using 20 series-connected TEG modules, and heat is dissipated through an aluminum heat exchanger. The system achieved 6.2 % efficiency with single-stage TEG, validating the integration of HPR and TEG technologies and enabling applications in underwater NUSTER systems. Data from HPTEG-1.0 has been used to optimize HPR systems [228–230].

HPTEG-2.0 [222] was designed to evaluate the integration of dynamic and static conversion technologies under higher power conditions for land-based applications. TEG, with its established research foundation, was chosen for static conversion, while the Stirling engine, which

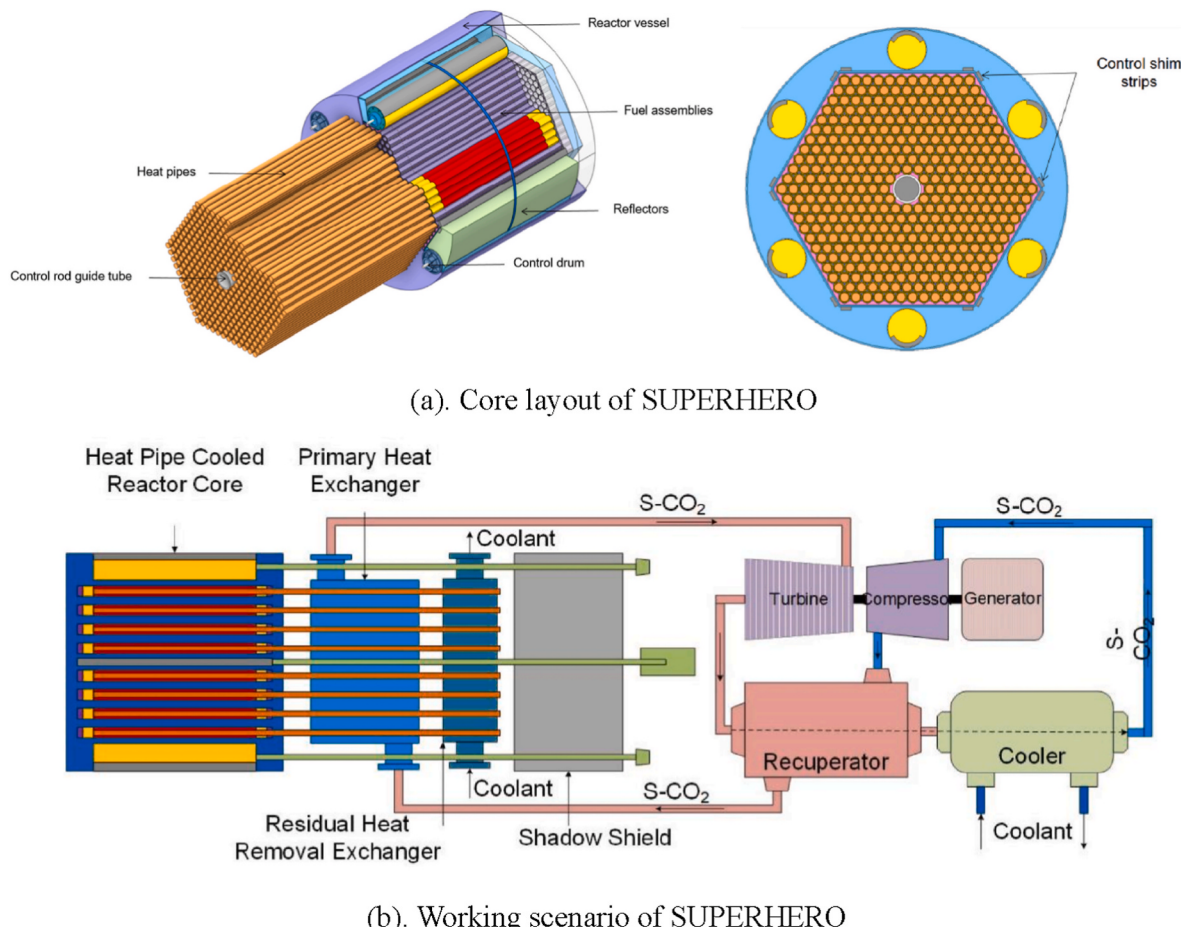


Fig. 29. Schematic design of SUPERHERO [49].

operates without an external circulation system, was selected for dynamic conversion. The system comprises three 1 kWe Stirling engines, 180 bismuth telluride TEUs, and 37 K-HTHPs, using 90 heating rods to simulate fuel rods with a rated power of 25 kWt (Fig. 32).

HPTEG-2.0 achieved a combined thermoelectric conversion efficiency of 16.7 %, below the expected 22 %. The shortfall was mainly attributed to a 340K temperature difference between the HTHP evaporator and the Stirling engine's hot end, highlighting the need for further optimization.

4.3.3. HPR-Brayton prototype

The integration of Brayton cycle technology with HPR represents a configuration with significant potential advantages. Numerous studies have proposed various applications suitable for this configuration, owing to the maturity of Brayton cycle technology and its theoretically straightforward coupling with HPRs. However, current research has primarily focused on theoretical analysis, such as the development of coupling models [51,231–233] and multi-objective optimization [234]. Experimental validation of the feasibility of integrating the Brayton cycle with HPRs remains scarce.

In this regard, Li et al. [235] established a coupling test system between HTHP and the Brayton cycle and investigated the load-following capability and efficiency variations of the Brayton system (Fig. 33). Deng et al. [236] established a coupling system between HTHP and an open Brayton cycle, obtaining valuable experimental data on the coupled system (Fig. 34).

5. Major issues in the application of HPR technology

Beyond advancements in fundamental design and theoretical development, several engineering issues have emerged in the practical application of HPRs, which were previously overlooked during the design phase. These issues primarily involve gaps in heat transfer failure mechanisms and modes, as well as unexpected design deviations caused by the strongly coupled multi-physics interactions inherent in HPRs. This section reviews these two aspects.

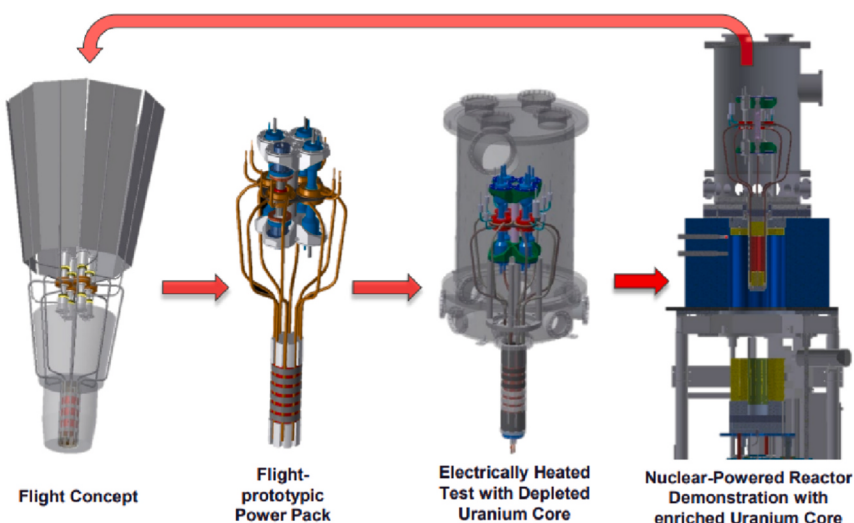
5.1. Heat transfer failure modes in HPR

Factors contributing to heat transfer failure in HPRs include corrosion, heat transfer limits, creep and rupture, and non-condensable gases. Based on these potential mechanisms, failure modes can be categorized into three main aspects: corrosion failure, heat transfer failure, and structural failure.

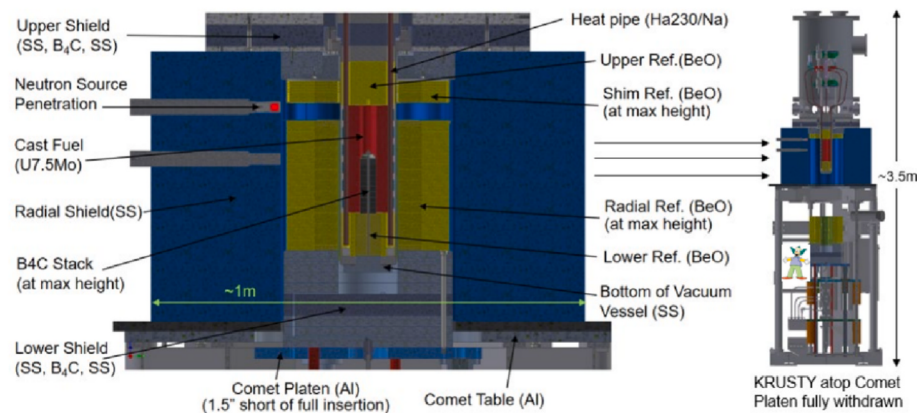
5.1.1. Corrosion failure

Corrosion failure primarily results from the corrosive effects of alkali metals [237], with the rate and severity depending on material compatibility. Corrosion forms microscopic pits on the material surface, which can propagate inherent cracks, eventually leading to rupture failure. Tu et al. [237] studied the mechanisms of corrosion failure and found that, although different materials exhibit varying resistance to alkali metal corrosion at high temperatures, the underlying mechanisms are similar, encompassing crevice corrosion, uniform corrosion, and grain boundary coarsening (Fig. 35).

Current research on corrosion failure in HPRs primarily focuses on



(a). KRUSTY development path



(b). KRUSTY configuration

Fig. 30. KRUSTY prototype testing [224].

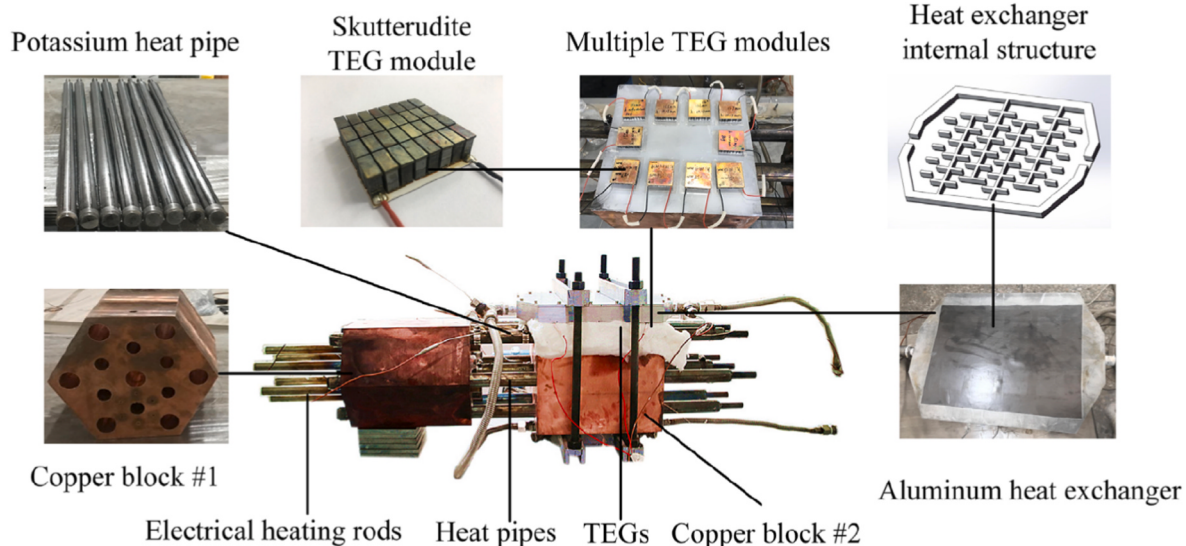


Fig. 31. HPTEG-1.0 prototype testing [227].

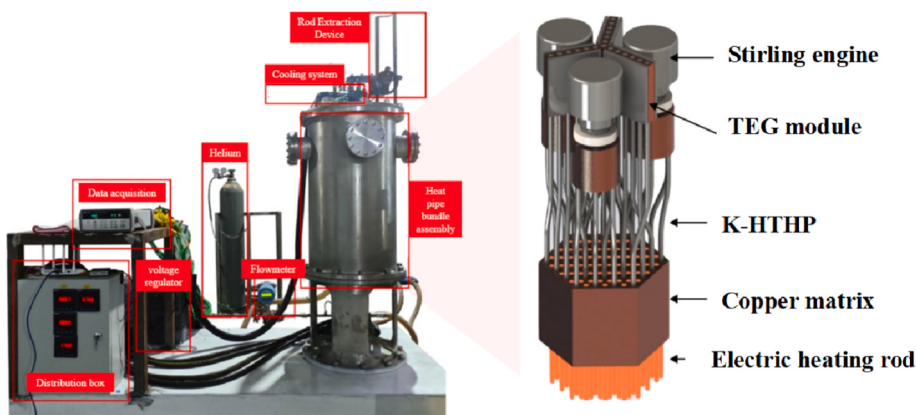


Fig. 32. HPTEG-2.0 prototype testing.



Fig. 33. Brayton cycle test loop established by Li et al. (EH: electric heater, RE: regenerator, TAC: turbine-alternator-compressor) [235].

experimentally measuring corrosion depths. For instance, Ewell et al. [238] tested a SS304-walled Na/K HTHP, Chen et al. [239] tested a GH181/1Cr18Ni9Ti-walled Na HTHP, Tu et al. [240] tested a 15CrMo/12CrMoV/1Cr18Ni9Ti-walled Na HTHP, and Jin et al. [241] studied a GH181-walled Na HTHP. However, the development of detailed theoretical frameworks to fully understand these mechanisms remains a gap requiring further research.

5.1.2. Heat transfer failure

Heat transfer failure occurs in HPRs when they reach heat transfer limit due to improper design or operating conditions, leading to material overheating or even burnout, often associated with the dry-out process [192]. Additionally, non-condensable gases play a significant role by preventing the condensation of working fluid vapor in the condenser [74], thereby obstructing return flow and degrading heat transfer performance.

Various heat transfer limits can typically be derived through theoretical analysis [72]. Current research focuses on improving and refining correction factors through experimental studies to adjust these heat transfer limits [68], making them applicable to a broader range of conditions.

In 2019, Sandia National Laboratory (SNL) conducted a deliberate dry-out test on a Na-HTHP and reported that the dry-out point significantly exceeded the predicted value [242], indicating traditional heat

transfer limit models are too conservative. In this context, Lee et al. [243] developed a capillary limit model incorporating filling ratio effects, improving the accuracy of dry-out point predictions and showing that overheated HTHPs can remain stable under certain conditions. This could be a key factor in future research on long, high-filling-ratio HTHPs. Additionally, Zhang et al. [244] revealed that non-condensable gases reduce heat transfer under choked flow conditions. Ma et al. [245] introduced a capillary evaporating film model to include microscopic forces in capillary action and experimentally measured the capillary limit [246]. These studies aim to update heat transfer limit theories to account for new phenomena observed in experiments but are limited to adding correction factors to existing formulas.

5.1.3. Structural failure

Structural failure in HPRs mainly occurs as high-temperature creep and thermal fatigue, representing the most severe failure type due to the complete loss of reactor functionality.

In the current studies, creep failure is often predicted using empirical or semi-empirical models, including the Paris law for crack fatigue growth rate [247], the Monkman-Grant equation for creep life [248], and the Larson-Miller Parameter (LMP) model for creep rupture time [249].

Thermal fatigue is largely attributed to heat transfer oscillations in HTHPs, characterized by periodic fluctuations in thermal parameters at specific power ranges (Fig. 36). These oscillations can cause power variations of approximately 10 % and significant stress fluctuations. Current research on heat transfer oscillations mainly focuses on low-temperature heat pipes, which differ from HTHPs in that they allow boiling, resulting in distinct initiation mechanisms. Numerous experiments on HTHPs [196–198,200] have observed heat transfer oscillations, but a comprehensive theory to explain this phenomenon remains lacking. Wang et al. [250] conducted 3D-CFD simulations of geyser boiling in HTHPs and successfully explained the mechanism of temperature oscillations induced by geyser boiling, providing valuable guidance for future research.

5.2. Multi-physical coupling analysis in HPR

5.2.1. Multi-physical fields overview

The strong interactions among neutronic, thermal, mechanical, and electrical processes in HPRs make multi-physics coupling an essential aspect, closely linked to their miniaturized design [16]. In conventional liquid-cooled reactors, multi-physics interactions are typically limited to neutron-thermal coupling, as mechanical and electrical effects can often be mapped to thermal effects in a unidirectional manner. However, in HPRs, significant thermal expansion induces changes in stress, density, contact thermal resistance, and system displacement, and causes more

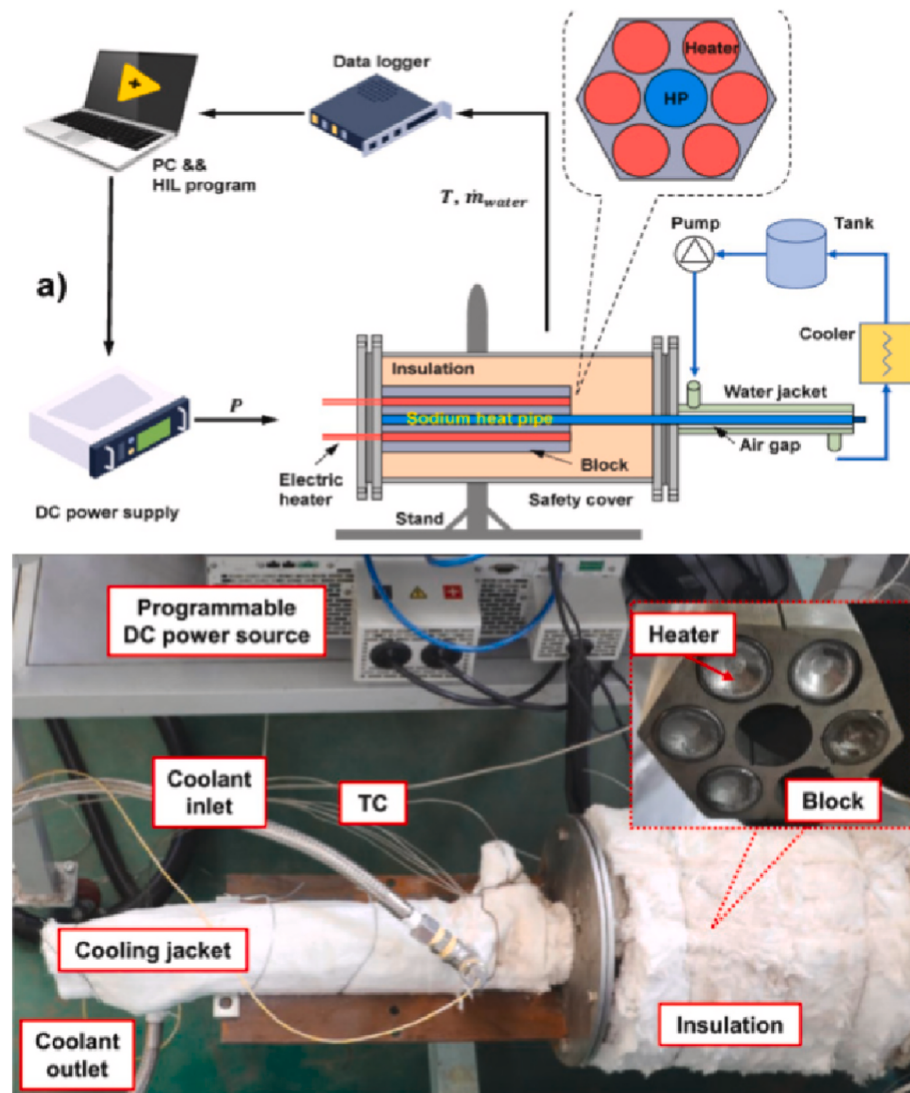


Fig. 34. Brayton cycle test loop established by Deng et al. (TC: thermocouple) [236].

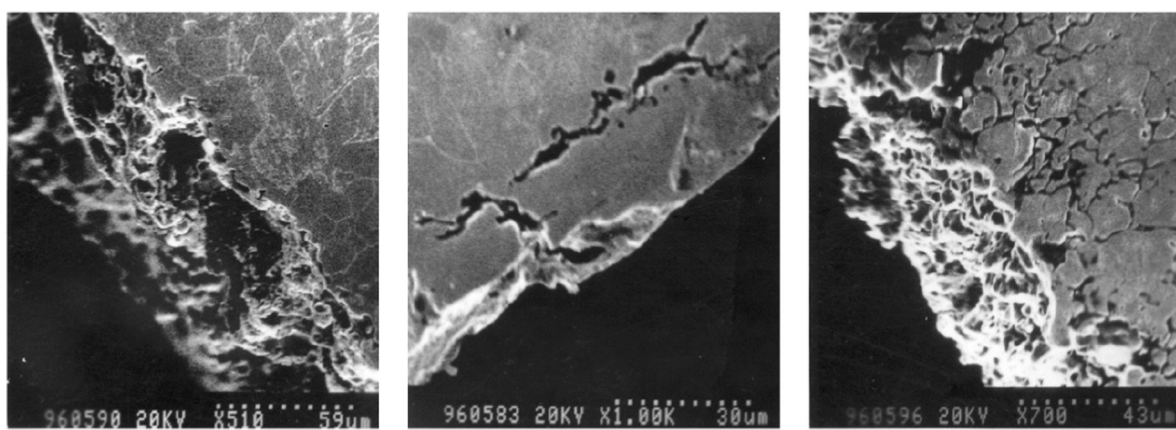


Fig. 35. Corrosion of metals by alkali metals: Crevice corrosion (left), Uniform corrosion (middle), Grain boundary coarsening (right) [237].

than 90 % of the reactivity feedback [251], which in turn affect other physical fields (Fig. 37), resulting in a complex overall response.

5.2.2. Existing coupling strategies

Currently, there is no fully integrated multi-physics coupling

framework for HPRs that can achieve complete internal coupling. In most studies, specialized software packages or self-coded codes are used for neutronic, thermal, mechanical, and electrical analyses. These are coupled through external iterations, with asynchronous data transfer interfaces between each component. Table 10 summarizes the latest

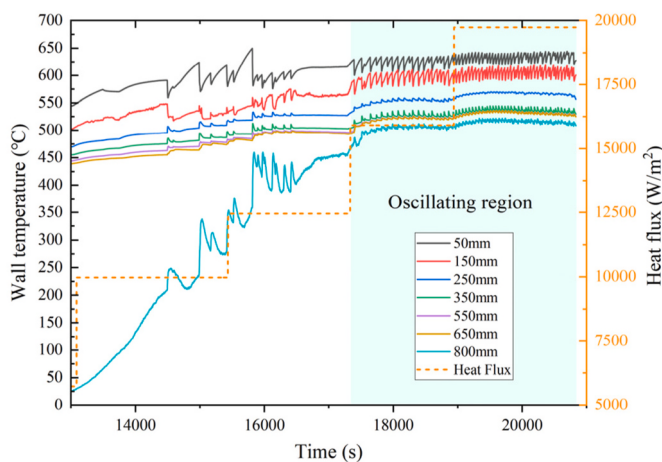


Fig. 36. Typical heat transfer oscillations in HTHP.

studies on HPR multi-physical coupling.

As shown in Table 10, there is currently no comprehensive framework capable of integrating and analyzing the impacts of neutronic, thermal, mechanical, and electrical factors. Most studies [239–251] overlook the influence of electrical effects on the overall coupling, which has been proven to significantly affect the transient thermal characteristics of the core [46]. The development of open-source platforms such as OpenFOAM and MOOSE offers a new approach to constructing a unified framework solver.

6. Recommendations for future trends of HPR technologies

HPRs have garnered widespread attention due to their potential for mobility, safety, and sustainability. Although significant progress has been made in research to date, there are still gaps that need to be addressed. Future development should emphasize innovations in design, material development, and installation and deployment strategies to meet the challenges of modern energy demands. Based on the current state of research, this paper proposes the following outlooks.

1) Promotion and application of LEU

Fuel enrichment is a key challenge for HPRs, especially with the need for miniaturization requiring higher levels. Most HPR designs currently use HEU, raising nuclear proliferation concerns and becoming a policy

issue [15]. For land- or sea-based HPRs, designs must align with international policies and security standards, complicating commercialization efforts.

As a candidate for power supply, neutron economy should still be considered, meaning that HPRs are not necessarily required to adopt a fast-spectrum design. The eVinci reactor utilizes TRISO fuel (19.75 % enrichment) combined with metal hydride moderation [14], presenting a novel and viable approach.

2) Redefinition of safety assessments

Mobile HPRs face complex operating conditions and harsh environments, with safety risks differing greatly from large commercial nuclear plants. Research on HPR accident progression, consequences, and countermeasures is limited.

Traditional liquid-cooled reactor safety systems, such as automatic depressurization and spray cooling, may not be suitable for HPRs. Additionally, accidents involving alkali metal reactions introduce new challenges, necessitating updated safety margin assessments and a revised concept of defense-in-depth. In particular, it is crucial to evaluate the possibility and consequences of secondary melt-through caused by alkali metal exposure and reactions.

3) Development and testing of high-temperature materials

HPRs operate at extremely high temperatures, imposing significant demands on structural materials due to thermal stresses from the solid-state core. Ni-based alloys like Haynes and Hastelloy N show promise with proven high-temperature and corrosion resistance but lack approval for nuclear use. Further refinement and long-term testing are needed to meet nuclear standards.

On the other hand, Ni-free ODS has emerged as a promising alternative, offering superior resistance to high temperatures and oxidation, as well as lower cost and improved manufacturability. However, precisely controlling the dispersion and distribution of oxide particles, along with long-term performance validation, remains a challenge that requires further investigation.

4) Unified framework for multi-physical coupling analysis

HPRs feature a compact design, small size, and rapid power adjustment capabilities, requiring a detailed study of their neutronic-thermal-mechanical-electrical multi-physics coupling framework. These interactions strongly influence safety analysis results. Traditional external coupling strategies face limitations, such as slow data exchange and

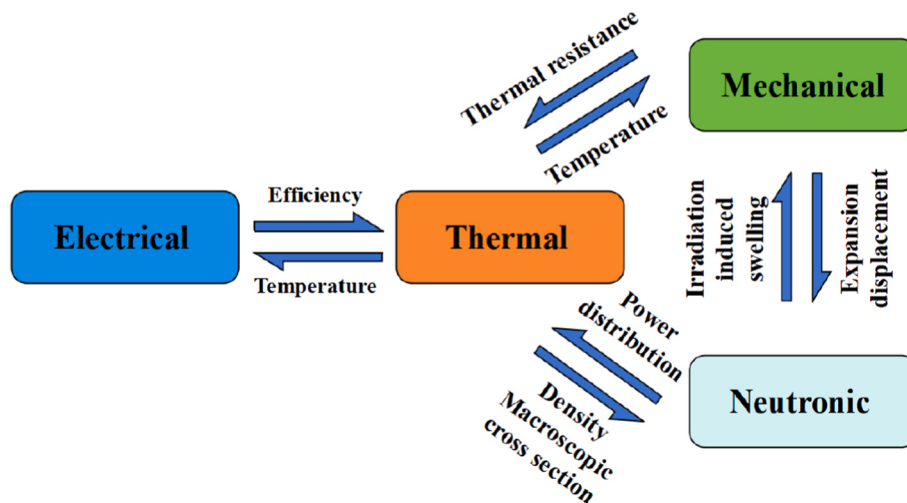


Fig. 37. General case of neutronic-thermal-mechanical-electrical multi-physics coupling.

Table 10

Studies on HPR multi-physics coupling analysis.

Ref.	Codes/Software used				Object	Multiphysics purpose
	Neutronic	Thermal	Mechanical	Electrical		
Li et al. [252]	Self-coded (D) in OpenFOAM	Self-coded (HFM) in OpenFOAM	–	Self-coded in OpenFOAM	HOMER-15	- N-T-E coupling - Load-following analysis
Wang et al. [253]	OpenMC (MC)	Self-coded (NTM)	Abaqus	–	Megapower	- N-T-M coupling - Influence of plastic deformation
Zhang et al. [254]	OpenMC (MC)	Nektar++ (HFM & FSM)	SfePy	–	Megapower	- N-T-M coupling - HTHP failure analysis
Ma et al. [255]	RMC (MC)	HPRTRA (NTM & FSM)	Ansys Mechanical	–	Megapower	- N-T-M coupling - HTHP failure analysis
Ma et al. [256]	RMC (MC)	HPRTRAN (NTM & FSM)	Ansys Mechanical	–	Megapower	- N-T-M coupling - Introduce irradiation effects
Lee and Jung [257]	PROTEUS (D)	ANLHTP (NTM)	–	–	Megapower	- N-T coupling - Single-HTHP-failure analysis
Guo et al. [258, 259]	RMC (MC)	Self-coded (NTM & FSM) in OpenFOAM	Built-in Modules of OpenFOAM	–	KRUSTY	- N-T-M coupling - Heat sink loss analysis
Jeong et al. [260]	PRAGMA (MC)	ANLHTP (NTM)	Built-in Modules of OpenFOAM	–	Megapower	- N-T-M coupling - Heat sink loss analysis
Xiao et al. [261]	OpenMC (MC)	Nektar++ (NTM)	SfePy	–	KRUSTY	- N-T-M coupling - HTHPs failure analysis
Wu et al. [262]	OpenMC (MC)	Self-coded (LM)	Built-in Modules of COMSOL	–	KRUSTY	- Burn-up effects analysis - N-T-M coupling - Steady-state analysis
Chen et al. [263]	OpenMC (MC)	Self-coded (NTM)	Built-in Modules of MOOSE	–	KRUSTY	- N-T-M coupling - Single-HTHP-failure analysis - Load-following analysis
Matthews et al. [264]	Griffin (D) & Serpent2 (MC)	Sockeye (NTM)	Bison	–	Empire	- N-T-M coupling - Formation of the DireWolf
Stauff et al. [265]	Griffin (D)	Sockeye (NTM)	Bison	–	HP-MR	- N-T-M coupling - Multi-condition validation
Zhang et al. [103]	SARAX (D)	HPSTAC (HFM & FSM)	–	HEART	NUSTER	- N-T-E coupling - HTHPs failure analysis

Notes.

In the "Neutronic" column: D - Deterministic method, MC - Monte Carlo method.

In the "Thermal" column: (Indicates HTHP model).

In the "Multiphysics purpose" column: N – Neutronic, T – Thermal, M – Mechanical, E – Electrical.

interface standard constraints. Recently, standardized CFD toolkits, such as MOOSE and OpenFOAM, have introduced new possibilities for unified and efficient multiphysics coupling analysis in HPRs.

Due to differences in data density, convergence criteria, and iterative schemes among various physical fields, two potential approaches exist. One approach is to compute the parameter distributions of all physical fields on a unified mesh, which requires the development of a complex and numerically stable multiphysics solver, making it highly challenging. Alternatively, a more promising approach is to construct individual solvers tailored to each physical field and perform mesh data mapping at given time steps, offering greater flexibility and computational efficiency.

5) In-loop testing of energy conversion systems

Energy conversion systems for HPRs face two main challenges: system performance and integration with HPR cores. Static systems, though suitable for HPRs, primarily face issues of material strength and lifespan. Dynamic systems, however, must address configuration, materials, efficiency, lifespan, and compatibility with HPR systems. Specific energy conversion systems must undergo in-loop testing to demonstrate their feasibility for coupling with HPRs. Given the qualification and safety concerns associated with nuclear-loaded tests, hardware-in-the-loop [236] testing presents a viable alternative, enabling the reproduction of a reactor's true behavior under temperature feedback conditions.

Additionally, integrating multiple energy conversion methods to

develop hybrid energy conversion systems for optimal energy utilization is a promising direction. Examples include combining AMTEC with TEG, Stirling engine with TEG, TIC with TPV, and the Brayton cycle with the Rankine cycle, among others.

6) Theoretical advancements and process improvements of HTHPs

Research on HTHPs largely focuses on experimental testing, with notable gaps in theoretical heat transfer and manufacturing. Manufacturing challenges include: (1) design, processing, and testing of wicking structures, (2) fabrication of high-temperature, corrosion-resistant pipes, (3) high-vacuum filling and sealing, (4) purification and compatibility of high-purity alkali metals, (5) precise assembly of wicks and pipes, and (6) development of process standards.

Research gaps in the HTHP theoretical models involve: (1) LVI migration, (2) alkali metal evaporation and condensation adjustment coefficient, (3) heat transfer oscillation, (4) probabilistic failure, (5) cascading failure, and (6) revisions to heat transfer limit theories.

7) Assembly and construction of HPR cores

A key challenge in manufacturing HPR cores lies in assembling the metal matrix with fuel rods and HTHPs. Designs often require hundreds or thousands of in-core fuel rods and HTHPs, with hard metal matrices demanding extremely precise drilling of holes with edge distances as small as 0.5 mm. Misalignment during assembly can introduce

mechanical stress, potentially compromising reactor safety. Casting techniques, while an alternative, may not provide sufficient strength. Future solutions may include integrated manufacturing, 3D printing technologies, and modular fuel designs, though issues like thermal expansion and component displacement require further study.

The modular manufacturing and assembly of fuel-HTHP units is a promising approach, but overcoming uneven thermal expansion caused by non-uniform temperature distribution remains a key challenge. Integrating Gen-IV reactor technologies with HPR designs to break through existing design bottlenecks could be a new direction. For instance, replacing the metallic matrix in HPRs with enclosed low-Prandtl-number fluids may offer advantages. Potential candidates include lead-bismuth eutectic (from lead-cooled fast reactors) or fluoride salts (from molten salt reactors), both of which have reached a considerable level of technological maturity, providing a novel pathway for HPR development.

7. Conclusions

The development of HPRs marks a major innovation in the nuclear energy sector, driven by the growing demand for efficient, safe, and sustainable energy solutions. From a design perspective, HPRs offer significant advantages over traditional reactors, particularly in simplicity, compactness, and passive safety. By utilizing heat pipes for core cooling, HPRs eliminate the need for mechanical pumps, reducing the likelihood of system failures and ensuring higher reliability, especially in remote or off-grid applications. This paper comprehensively reviews the development, challenges, research status, and future outlook of HPR technology. The key conclusions are as follows.

- 1) Since the 1960s, HPR designs have undergone continuous evolution and development. Technological advancements have led to more complex structures, higher reliability, greater power output, and enhanced application flexibility. The successful demonstration of the KRUSTY prototype marks the transition of HPRs from conceptual design to practical engineering applications. Their deployment in distributed energy systems, such as space exploration and mobile nuclear power solutions, highlights their potential to meet increasing energy demands while minimizing environmental impact.
- 2) Most HPRs currently utilize HEU fast-spectrum cores to meet miniaturization requirements. However, this approach increases shielding and reflection needs, reduces neutron economy, and raises proliferation concerns, complicating further deployment. As a result, core configuration is a crucial factor in HPR development, with a future trend shifting toward LEU designs. The successful implementation of TRISO fuel presents a viable alternative for future applications.
- 3) This study categorizes HPR-compatible energy conversion systems into dynamic and static types and reviews their respective principles and structures. The selection of an appropriate energy conversion system depends on specific application requirements, considering factors such as conversion efficiency, spatial utilization, and power range. A major bottleneck in existing energy conversion systems is poor material durability, resulting in short lifetimes that do not align with the lifespan of nuclear systems. A promising direction is the integration of multiple energy conversion technologies to enhance overall performance.
- 4) HTHPs are critical components in HPRs, directly influencing the thermal characteristics of the entire system. Advanced experimental techniques, such as intrusive measurements and X-ray imaging, have revealed new two-phase heat and mass transfer phenomena inside HTHPs, including heat transfer oscillations and flow pattern evolution. However, theoretical studies still lack a comprehensive framework to explain these observations. Current HTHP research remains at the macroscopic level, with limited understanding of heat and

mass transfer mechanisms at the microscale within the porous wick structure, presenting a major gap in the field.

- 5) Heat transfer failure and multiphysics coupling present major engineering challenges in HPR applications. While significant progress has been made in understanding failure modes, there is still no comprehensive theoretical framework to predict corrosion failure, heat transfer failure, and structural failure in HPRs. Additionally, in multiphysics coupling, current external coupling studies lack a consensus on coupling strategies. The development of a unified framework for analyzing these interactions represents a crucial future research direction.

Overall, HPRs hold immense potential for future energy applications. Future research should focus on optimizing core configurations, advancing HTHP theoretical models and experimental studies, and exploring innovative energy conversion technologies to improve system efficiency. As HPR technology matures, addressing these challenges will unlock its full potential, contributing to the development of sustainable, efficient, and safe nuclear power for the future.

Declaration of competing interest

The authors declare the following financial interests/personal relationships which may be considered as potential competing interests: Suizheng Qiu reports financial support was provided by National Natural Science Foundation of China.

Acknowledgments

This research is carried out under the financial support of the National Natural Science Foundation of China (Grant No. U2067208).

Appendix A. Supplementary data

Supplementary data to this article can be found online at <https://doi.org/10.1016/j.rser.2025.115486>.

Data availability

Data will be made available on request.

References

- [1] International Atomic Energy Agency. Nuclear energy makes history as final COP28 agreement calls for faster deployment. IAEA; 2024, July 28. Retrieved from, <https://www.iaea.org/newscenter/news/nuclear-energy-makes-history-as-final-cop28-agreement-calls-for-faster-deployment>.
- [2] Subki H. Advances in small modular reactor technology developments. 2020.
- [3] NEA. Small modular reactors challenges and opportunities. TechnicaIParis: OECD Publishing; 2021. Report No.:NEA No. 7560.
- [4] Wang C, Sun H, Tang S, Tian W, Qiu S, Su G. Thermal-hydraulic analysis of a new conceptual heat pipe cooled small nuclear reactor system. Nucl Eng Technol 2020;52(1):19–26.
- [5] Huang J, Wang C, Tian Z, Guo K, Su GH, Tian W, Qiu S. Preliminary conceptual design and analysis of a 100 kW level nuclear silent thermal-electrical reactor (NUSTER-100). Int J Energy Res 2022;46(14):19653–66.
- [6] Mason L, Poston D. A summary of NASA architecture studies utilizing fission surface power technology. In: 46th AIAA/ASME/SAE/ASEE joint propulsion conference & exhibit; 2011, April. p. 6599.
- [7] Lane TG, Revankar ST. Advances in technology, design and deployment of microreactors-a review. Prog Nucl Energy 2025;178:105520.
- [8] Hedayat A. A review of advanced Small Modular Reactors (SMRs) through a developed PIRT methodology. Radiation Physics and Engineering 2024;5(1): 21–39.
- [9] Deng J, Guan C, Sun Y, Liu X, Zhang T, He H, Chai X. Techno-economic analysis and dynamic performance evaluation of an integrated green concept based on concentrating solar power and a transportable heat pipe-cooled nuclear reactor. Energy 2024;132022.
- [10] Palac D, Gibson M, Mason L, Houts M, McClure P, Robinson R. Nuclear systems kilopower overview. 2016 (No. GRC-E-DAA-TN29740).
- [11] McClure PR, Poston DL, Dixon DD. Final results of demonstration using Flattop fissions (DUFF) experiment (No. LA-UR-12-25165). Los Alamos, NM (United States): Los Alamos National Lab.(LANL); 2012.

- [12] Briggs MH, Gibson MA, Sanzi JL. Electrically heated testing of the Kilowatt Reactor Using Stirling Technology (KRUSTY) experiment using a depleted uranium core. In: AIAA Propulsion and energy Forum and Exposition (No. NASA/TM-2018-219702); 2018, February.
- [13] Poston DI, Gibson MA, Sanchez RG, McClure PR. Results of the KRUSTY nuclear system test. *Nucl Technol* 2020;206(sup1):S89–117.
- [14] Swartz MM, Byers WA, Lojek J, Blunt R. Westinghouse eVinci™ heat pipe micro reactor technology development. International Conference on nuclear engineering, vol. 85246. American Society of Mechanical Engineers; 2021, August, V001T04A018.
- [15] Yan BH, Wang C, Li LG. The technology of micro heat pipe cooled reactor: a review. *Ann Nucl Energy* 2020;135:106948.
- [16] Bo W, Shunhao X, Bin W, Weibing W, Yongchao L, Tong L, Mengyao W. Review of recent research on heat pipe cooled reactor. *Nucl Eng Des* 2023;415:112679.
- [17] Voss SS. SNAP (Space Nuclear Auxiliary Power) reactor overview. Final Report No. AFWL-TN-84-14. Air Force Weapons Laboratory, Kirtland Air Force Base. 1984.
- [18] Johnson RA, Morgan WT, Rocklin SR. Design, ground test and flight test of SNAP 10A, first reactor in space. *Nucl Eng Des* 1967;5(1):7–21.
- [19] Ponomarev-Stepnoi NN, Kukharkin NE, Usov VA. "Romashka" reactor-converter. *Atom Energy* 2000;88(3):178–83.
- [20] Wiedemann C, Oswald M, Stabroth S, Klinkrad H, Vörsmann P. Size distribution of NaK droplets released during RORSAT reactor core ejection. *Adv Space Res* 2005;35(7):1290–5.
- [21] Stanculescu A. The role of nuclear power and nuclear propulsion. The peaceful exploration of space, vol. 1197. IAEA; 2005.
- [22] El-Genk MS. Deployment history and design considerations for space reactor power systems. *Acta Astronaut* 2009;64(9–10):833–49.
- [23] Voss SS. TOPAZ II system description (No. LA-UR-94-4). Los Alamos National Lab. 1994.
- [24] Tang S, Sun H, Wang C, Tian W, Qiu S, Su GH, Liu T. Transient thermal-hydraulic analysis of thermionic space reactor TOPAZ-II with modified RELAP5. *Prog Nucl Energy* 2019;112:209–24.
- [25] Reid RS, Merrigan MA, Sena JT. Review of liquid metal heat pipe work at Los Alamos. In: AIP conference proceedings, vol. 217. American Institute of Physics; 1991, January. p. 999–1008. 3.
- [26] Nasa N. NASA technology roadmaps TA 3: space power and energy storage. NASA Technol, Roadmaps 2015;2020:158–65. 117–121.
- [27] Miranda D. NASA technology taxonomy. Report No. HQ-E-DAA-TN76545. Washington, DC: NASA Headquarters; 2020.
- [28] Poston DI. The heatpipe-operated Mars exploration reactor (HOMER). In: AIP conference proceedings, vol. 552. American Institute of Physics; 2001, February. p. 797–804. 1.
- [29] Lambert T, Gilman P, Lilienthal P. Micropower system modeling with HOMER. Integration of alternative sources of energy 2006;1(1):379–85.
- [30] Yu H, Zhang Z, Chai X, Ma Y. Initiation and development of heat pipe cooled reactor. *Nucl Power Eng* 2019;40(4):1–8.
- [31] El-Genk MS, Tournier JMP. "SAIRS"-scalable Amtec integrated reactor space power system. *Prog Nucl Energy* 2004;45(1):25–69.
- [32] El-Genk MS, Tournier JM. Conceptual design of HP-STMCs space reactor power system for 110 kW_e. In: AIP conference proceedings, vol. 699. American Institute of Physics; 2004, February. p. 658–72. 1.
- [33] Tournier JM, El-Genk MS. Reactor lithium heat pipes for HP-STMCs space reactor power system. In: AIP conference proceedings, vol. 699. American Institute of Physics; 2004, February. p. 781–92. 1.
- [34] El-Genk MS, Tournier JM. Performance analysis of potassium heat pipes radiator for HP-STMCs space reactor power system. In: AIP conference proceedings, vol. 699. American Institute of Physics; 2004, February. p. 793–805. 1.
- [35] Liu X, Zhang R, Liang Y, Tang S, Wang C, Tian W, Su G. Core thermal-hydraulic evaluation of a heat pipe cooled nuclear reactor. *Ann Nucl Energy* 2020;142:107412.
- [36] Bushman A, Carpenter DM, Ellis TS, Gallagher SP, Herscovitch MC, Hine MC, et al. The Martian surface reactor: An advanced nuclear power station for manned extraterrestrial exploration. Report No. MIT-NSA-TR-003. Massachusetts Institute of Technology. 2004.
- [37] McClure PR, Poston DI, Dasari VR, Reid RS. Design of megawatt power level heat pipe reactors. USA: Report of Los Alamos National Laboratory; 2015.
- [38] Palac D, Gibson M, Mason L, Houts M, McClure P, Robinson R. Nuclear systems kilopower overview. 2016 (No. GRC-E-DAA-TN29740).
- [39] Ashcroft J, Eshelman C. Summary of NR program Prometheus efforts. In: AIP conference proceedings, vol. 880. American Institute of Physics; 2007, January. p. 497–521. 1.
- [40] Mason L, Poston D, Qualls L. System concepts for affordable fission surface power. In: Space technology and applications international Forum (STAIF 2008); 2008, January. No. NASA/TM-2008-215166.
- [41] McClure PR, Poston DI, Gibson MA, Mason LS, Robinson RC. Kilopower project: the KRUSTY fission power experiment and potential missions. *Nucl Technol* 2020;206(sup1):S1–12.
- [42] Poston DI, Gibson MA, McClure PR, Sanchez RG. Results of the KRUSTY warm critical experiments. *Nucl Technol* 2020;206(sup1):S78–88.
- [43] Zhang Z, Wang C, Guo K, Qiu S, Su GH, Tian W. Microreactors. In: Nuclear power reactor designs. Academic Press; 2024. p. 309–47.
- [44] Poston DI, Kapernick RJ, Guffee RM, Reid RS, Lipinski RJ, Wright SA, Talandis RA. Design of a heatpipe-cooled Mars-surface fission reactor. In: AIP conference proceedings, vol. 608. American Institute of Physics; 2002, January. p. 1096–106. 1.
- [45] Amiri BW, Sims BT, Poston DI, Kapernick RJ. A stainless-steel, uranium-dioxide, potassium-heatpipe-cooled surface reactor. In: AIP conference proceedings, vol. 813. American Institute of Physics; 2006, January. p. 289–97. 1.
- [46] Zhang Z, Wang C, Guo K, Huang J, Qiu S, Su GH, Tian W. HEART, a specific code for thermal-electrical analysis of heat pipe cooled nuclear reactor. *Int J Therm Sci* 2022;179:107666.
- [47] Zhang Z, Li P, Wang C, Guo K, Tian W, Qiu S, Su GH. Conceptual design of a mobile nuclear-electric hybrid energy storage system based on the heat pipe-cooled reactor. *Nucl Eng Des* 2024;424:113289.
- [48] Guo Y, Guo X, Guo S, Jiang H, Su Z, Wang G, Yu J. Conceptual design of megawatt-level mobile nuclear power system based on heat pipe cooled reactor. *Nucl Eng Des* 2023;413:112558.
- [49] Guo S, Guo X, Wang G, Guo Y, Wang Z, Leng J, Qian D. Conceptual design of a novel megawatt portable nuclear power system by supercritical carbon dioxide Brayton cycle coupled with heat pipe cooled reactor. *International Journal of Advanced Nuclear Reactor Design and Technology* 2023;5(4):168–88.
- [50] Zhang W, Zhang D, Wang C, Tian W, Qiu S, Su GH. Conceptual design and analysis of a megawatt power level heat pipe cooled space reactor power system. *Ann Nucl Energy* 2020;144:107576.
- [51] Cui DY, Dai Y, Cai XZ, Fu Y, Li XX, Zou Y, Chen JG. Preconceptual nuclear design of a 50 kW_t heat pipe cooled micro molten salt reactor (micro-MSR). *Prog Nucl Energy* 2021;134:103670.
- [52] Poston DI, Marcille TF, Kapernick RJ, Hiatt MT, Amiri BW. Evaluation of metal-fueled surface reactor concepts. In: AIP conference proceedings, vol. 880. American Institute of Physics; 2007, January. p. 149–56. 1.
- [53] Schriener TM, El-Genk MS. Effects of decreasing fuel enrichment on the design of the Pellet Bed Reactor (PeBR) for lunar outposts. *Prog Nucl Energy* 2018;104:288–97.
- [54] Fink JK. Thermophysical properties of uranium dioxide. *J Nucl Mater* 2000;279(1):1–18.
- [55] Brown NR, Aronson A, Todosow M, Brito R, McClellan KJ. Neutronic performance of uranium nitride composite fuels in a PWR. *Nucl Eng Des* 2014;275:393–407.
- [56] Vasudevanurthy G, Nelson AT. Uranium carbide properties for advanced fuel modeling—A review. *J Nucl Mater* 2022;558:153145.
- [57] Galahom AA. Improving the neutronic characteristics of a boiling water reactor by using uranium zirconium hydride fuel instead of uranium dioxide fuel. *Nucl Eng Technol* 2016;48(3):751–7.
- [58] Sinha VP, Prasad GJ, Hegde PV, Keswani R, Basak CB, Pal S, Mishra GP. Development, preparation and characterization of uranium molybdenum alloys for dispersion fuel application. *J Alloys Compd* 2009;473(1–2):238–44.
- [59] Brown NR. A review of in-pile fuel safety tests of TRISO fuel forms and future testing opportunities in non-HTGR applications. *J Nucl Mater* 2020;534:152139.
- [60] Jiang D, Zhang D, Li X, Wang S, Wang C, Qin H, Qiu S. Fluoride-salt-cooled high-temperature reactors: review of historical milestones, research status, challenges, and outlook. *Renew Sustain Energy Rev* 2022;161:112345.
- [61] Du X, Tao Y, Zheng Y, Wang C, Wang Y, Qiu S, Zhang B. Reactor core design of UPR-s: a nuclear reactor for silence thermoelectric system NUSTER. *Nucl Eng Des* 2021;383:111404.
- [62] Poston DI, Dixon DD, McClure PR, Gibson MA. A simple, low-power fission reactor for space exploration power systems. *Proc. of Nucl. and Emerging Tech. for Space* 2013:25–8.
- [63] Simnad MT. Nuclear reactor materials and fuels. 2002.
- [64] Poston DI, Marcille TF, Kapernick RJ, Hiatt MT, Amiri BW. Evaluation of metal-fueled surface reactor concepts. In: AIP conference proceedings, vol. 880. American Institute of Physics; 2007, January. p. 149–56. 1.
- [65] Wang YP, Tao YS, Wu YQ, Zhang YQ, Du XN. Shielding design of a megawatt-scale heat pipe reactor core. *Nucl Tech* 2023;46(2):020606.
- [66] Li F, Zheng Y, Tao Y. Radiation field analysis of a heat pipe cooled reactor for underwater application. In: Proceedings of the reactor physics Asia 2023 (RPHA2023) conference; 2023, October. Gyeongju, Korea.
- [67] Zhang Z, Zhao H, Wang C, Guo K, Su G, Tian W, Qiu S. Study on the start-up characteristics of a 100kWe-level nuclear silent heat pipe cooled reactor based on cascaded control. *Energy* 2025;314:134260.
- [68] Tian Z, Wang C, Guo K, Zhang D, Su GH, Tian W, Qiu S. A review of liquid metal high temperature heat pipes: theoretical model, design, and application. *Int J Heat Mass Tran* 2023;214:124434.
- [69] Khalid SU, Babar H, Ali HM, Janjua MM, Ali MA. Heat pipes: progress in thermal performance enhancement for microelectronics. *Journal of Thermal Analysis and Calorimetry* 2021;143:2227–43.
- [70] Jouhara H, Reay D, McGlen R, Kew P, McDonough J. Heat pipes: theory, design and applications. Butterworth-Heinemann; 2023.
- [71] Jouhara H, Chauhan A, Nannou T, Almahmoud S, Delpech B, Wrobel LC. Heat pipe based systems—Advances and applications. *Energy* 2017;128:729–54.
- [72] Chen Q, Zhou J, Zhou G, Cheng K, Huai X, Wei G. A comprehensive review of thermal performance improvement of high-temperature heat pipes. *J Therm Sci* 2024;33(2):625–47.
- [73] Mantelli MBH. Thermosyphons and heat pipes: theory and applications1. Switzerland: Springer International Publishing; 2021. p. 1–413.
- [74] Wang C, Zhang Z, Zhang M, Li P, Tian Z, Tian W, Su GH. Numerical evaluation of non-condensable gas influence on the heat transfer characteristics of high-temperature lithium heat pipe during reactor operation. *Ann Nucl Energy* 2022;173:109077.
- [75] Martin WR, Weir JR. Effect of elevated-temperature irradiation on Hastelloy N. *Nucl Appl* 1965;1(2):160–7.

- [76] Surenkov AI, Ignatiev VV, Trun'kin IN, Presnyakov MY, Uglov VS. Investigation of the corrosion resistance of nickel-molybdenum alloys in the eutectic LiF-NaF-KF. Atom Energy 2021;129:135–40.
- [77] Liu Q, Leng B, Qiu J, Yin H, Lin J, Tang Z. Effect of graphite particles in molten LiF-NaF-KF eutectic salt on corrosion behaviour of GH3535 alloy. Corros Sci 2020;168:108581.
- [78] Li H, Zheng W, Du B, Yin H, He X, Ma T, Yang X. The high temperature corrosion of Incoloy 800H alloy at three different atmospheres. J Nucl Sci Technol 2023;60(2):165–74.
- [79] Tung HM, Mo K, Stubbins JF. Biaxial thermal creep of inconel 617 and Haynes 230 at 850 and 950° C. J Nucl Mater 2014;447(1–3):28–37.
- [80] Chomette S, Gentzbittel JM, Viguer B. Creep behaviour of as received, aged and cold worked INCONEL 617 at 850 C and 950 C. J Nucl Mater 2010;399(2–3):266–74.
- [81] Kumar AS, Sharma SK, Shukla AK. Microstructural, mechanical, and thermal analysis of SS316L weldment for marine engineering application. J Mater Eng Perform 2023;1–14.
- [82] Field KG, Snead MA, Yamamoto Y, Terrani KA. Handbook on the material properties of FeCrAl alloys for nuclear power Production applications (FY18 Version: Revision 1) (No. ORNL/SPR-2018/905). Oak Ridge, TN (United States): Oak Ridge National Lab.(ORNL); 2018.
- [83] Rajesh VG, Ravindran KP. Optimum heat pipe design: a nonlinear programming approach. Int Commun Heat Mass Tran 1997;24(3):371–80.
- [84] Tian Z, Liu Y, Wang C, Guo K, Zhang D, Tian W, Su GH. Single/multi-objective optimization and comparative analysis of liquid-metal heat pipe. Int J Energy Res 2022;46(12):17521–39.
- [85] Hu H, Zhao Y, Li Y. Research progress on flow and heat transfer characteristics of fluids in metal foams. Renewable and sustainable energy reviews 2023;171:113010.
- [86] Xu ZG, Zhao CY. Experimental study on pool boiling heat transfer in gradient metal foams. Int J Heat Mass Tran 2015;85:824–9.
- [87] Li Z, Juxiang L, Mian Z. Heat transfer of porous metal foam wick heat pipe. CIESC Journal 2011;63(12):3861–6.
- [88] Somasundaram D, Mani A, Kamaraj M. Experimental investigation of thermal performance of metal foam wicked flat heat pipe. Exp Therm Fluid Sci 2017;82:482–92.
- [89] Shen L, Xu S, Bai Z, Wang Y, Xie J. Experimental study on thermal and flow characteristics of metal foam heat pipe radiator. Int J Therm Sci 2021;159:106572.
- [90] Manova S, Asirvatham LG, Angeline AA, Jerbin S, Bose JR, Nimmagadda R, Wongwises S. Comparison on the heat transfer performance and entropy analysis on miniature loop thermosyphon with screen mesh wick and metal foam. Case Stud Therm Eng 2022;38:102310.
- [91] Hansen G, Næss E, Kristjansson K. Analysis of a vertical flat heat pipe using potassium working fluid and a wick of compressed nickel foam. Energies 2016;9(3):170.
- [92] Champier D. Thermoelectric generators: a review of applications. Energy Convers Manag 2017;140:167–81.
- [93] Go DB, Haase JR, George J, Mannhart J, Wanke R, Nojeh A, Nemanich R. Thermionic energy conversion in the twenty-first century: advances and opportunities for space and terrestrial applications. Front Mech Eng 2017;3:13.
- [94] El-Genk MS, Tournier JM. High power AMTEC converters for deep-space nuclear reactor power systems. Expanding the Frontiers of Space 2003;654:730–9.
- [95] Wilt DM, Chubb DL. A review of recent thermophotovoltaic energy conversion technology development at NASA Lewis Research Center. In: AIP conference proceedings, vol. 420. American Institute of Physics; 1998, January. p. 1410–6. 1.
- [96] Bera TK, Bohre AK, Ahmed I, Bhattacharya A, Bhowmik PS. Magnetohydrodynamic (MHD) power generation systems. In: Planning of hybrid renewable energy systems, electric vehicles and microgrid: modeling, control and optimization. Singapore: Springer Nature Singapore; 2022. p. 905–29.
- [97] Thaikattil GJ, Sanzi JL, Goodell D, Barth C, Gibson M. Consolidation of A Sodium heat pipe and stirling engine for fission surface power. In: Thermal fluids analysis Workshop (TFAWS); 2023, August.
- [98] Yu GP, Cheng YF, Zhang N, Ming PJ. Multi-objective optimization and evaluation of supercritical CO₂ Brayton cycle for nuclear power generation. Nucl Sci Tech 2024;35(2):22.
- [99] Angelo Jr J, Buden D. Space nuclear power. 1985.
- [100] Hadjistassou C, Kyriakides E, Georgiou J. Designing high efficiency segmented thermoelectric generators. Energy Convers Manag 2013;66:165–72.
- [101] Pei J, Li L, Liu D, Zhang B, Xiao Y, Li J. Development of integrated two-stage thermoelectric generators for large temperature difference. Sci China Technol Sci 2019;62(9):1596–604.
- [102] He Z, Yang M, Wang Z, Chen H, Zhang X, Jiang Q, Zhang H. Optimization of segmented thermoelectric devices composed of high-temperature thermoelectric material La₂Te₃. Advanced Composites and Hybrid Materials 2022;5(4):2884–95.
- [103] Zhang Z, Wang C, Tan C, Guo K, Su G, Tian W, Qiu S. Investigation of neutronic and thermal-electric coupling phenomenon in a 100 kW_e-level nuclear silent heat pipe-cooled reactor. Appl Therm Eng 2024;236:121765.
- [104] Mukherjee M, Srivastava A, Singh AK. Recent advances in designing thermoelectric materials. J Mater Chem C 2022;10(35):12524–55.
- [105] Zhao C, Li Y, Liu Y, Xie H, Yu W. A critical review of the preparation strategies of thermally conductive and electrically insulating polymeric materials and their applications in heat dissipation of electronic devices. Advanced Composites and Hybrid Materials 2023;6(1):27.
- [106] Wang X, Sheng Y, Ning J, Xi J, Xi L, Qiu D, Ke X. A critical review of machine learning techniques on thermoelectric materials. J Phys Chem Lett 2023;14(7):1808–22.
- [107] Wang T, Zhang C, Snoussi H, Zhang G. Machine learning approaches for thermoelectric materials research. Adv Funct Mater 2020;30(5):1906041.
- [108] Jaafreh R, Seong KY, Kim JG, Hamad K. A deep learning perspective into the figure-of-merit of thermoelectric materials. Mater Lett 2022;319:132299.
- [109] Dai Z, Wang C, Zhang D, Tian W, Qiu S, Su G. Thermoelectric characteristics analysis of thermionic space nuclear power reactor. Int J Energy Res 2020;44(2):855–68.
- [110] Wuye ZHONG, Shouzhi ZHAO, Jianping ZHENG, Zheng LV, Jiachun XIE. A review of technology development of thermionic energy conversion for space application. Journal of Deep Space Exploration 2020;7(1):47–60.
- [111] Mukherjee M, Srivastava A, Singh AK. Recent advances in designing thermoelectric materials. J Mater Chem C 2022;10(35):12524–55.
- [112] Lee JH, Bargatin I, Vancil BK, Gwinn TO, Maboudian R, Melosh NA, Howe RT. Microfabricated thermally isolated low work-function emitter. J Microelectromech Syst 2014;23(5):1182–7.
- [113] Paxton WF, Wisitsoraat A, Raina S, Davidson JL, Kang WP, P2. 14: characterization of the thermionic electron emission properties of nitrogen-incorporated “ridged” nanodiamond for use in thermal energy conversion. In: International vacuum Nanoelectronics conference. IEEE; 2010, July. p. 149–50.
- [114] Westover TL, Franklin AD, Cola BA, Fisher TS, Reifenberger RG. Photo-and thermionic emission from potassium-intercalated carbon nanotube arrays. J Vac Sci Technol B 2010;28(2):423–34.
- [115] Michel JA, Robinson VS, Yang L, Sambandam S, Lu W, Westover T, Lukehart CM. Synthesis and characterization of potassium metal/graphitic carbon nanofiber intercalates. J Nanosci Nanotechnol 2008;8(4):1942–50.
- [116] Lee WH, Hwang HC, Lee JS, Kim PJ, Lim SH, Rhi SH, Lee KW. Study on the characteristics of an alkali-metal thermoelectric power generation system. J Electron Mater 2015;44:3534–44.
- [117] Lodhi MAK, Vijayaraghavan P, Daloglu A. An overview of advanced space/terrestrial power generation device: AMTEC. J Power Sources 2001;103(1):25–33.
- [118] Alger DL. Some corrosion failure mechanisms of AMTEC cells. In: IECEC-97 proceedings of the Thirty-Second Intersociety energy conversion engineering conference (Cat. No. 97CH6203), vol. 2. IEEE; 1997, July. p. 1224–9.
- [119] Zhou Y, Zhang S, Li G. A review of radioisotope batteries. Chin Sci Bull 2017;62(17):1831–45.
- [120] Miao X, Zhang H, Ma F, Deng M, You E. Performance evaluation of AMTEC/TEG coupling system for nuclear power space stations in space exploration. Ann Nucl Energy 2024;207:110742.
- [121] Bauer T. Thermophotovoltaics: basic principles and critical aspects of system design. Springer Science & Business Media; 2011.
- [122] Bauer T. Thermophotovoltaics: basic principles and critical aspects of system design. Springer Science & Business Media; 2011.
- [123] Bellucci A, García-Linares P, Martí A, Trucchi DM, Datas A. A three-terminal hybrid thermionic-photovoltaic energy converter. Adv Energy Mater 2022;12(20):2200357.
- [124] Datas A, Vaillon R. Thermionic-enhanced near-field thermophotovoltaics. Nano Energy 2019;61:10–7.
- [125] Bera TK. A magnetohydrodynamic (MHD) power generating system: a technical review. In: IOP conference series: materials Science and engineering, vol. 955. IOP Publishing; 2020, November, 012075. No. 1.
- [126] Litchford RJ, Harada N. Multi-MW closed cycle MHD nuclear space power via nonequilibrium He/Xe working plasma. 2011. No. Paper 3349.
- [127] Kayukawa N. Open-cycle magnetohydrodynamic electrical power generation: a review and future perspectives. Prog Energy Combust Sci 2004;30(1):33–60.
- [128] Luchinkin NA, Razuvanov NG, Polyanskaya ON, Sokolov MA, Burdyukova EA. Heat transfer in a liquid metal upflow in a pipe with mixed turbulent convection complicated by the influence of magnetic field. J Eng Phys Thermophys 2022;95(6):1548–59.
- [129] Kongtragoon B, Wongwises S. A review of solar-powered Stirling engines and low temperature differential Stirling engines. Renewable and Sustainable energy reviews 2003;7(2):131–54.
- [130] Toro C, Lior N. Analysis and comparison of solar-heat driven Stirling, Brayton and Rankine cycles for space power generation. Energy 2017;120:549–64.
- [131] Wang H, Chen Y, Luo J, Zhang L, Kang H, Luo E, Zhu S. A novel high-power free-piston stirling engine generator with integrated heat pipes for thermal-to-electric conversion of clean energy. Energy 2025;314:134218.
- [132] Andreades C, Dempsey L, Peterson PF. Reheat air-brayton combined cycle power conversion off-nominal and transient performance. J Eng Gas Turbines Power 2014;136(7):071703.
- [133] Biondi A, Toro C. Closed Brayton cycles for power generation in space: modeling, simulation and exergy analysis. Energy 2019;181:793–802.
- [134] Tian Z, Jiang B, Malik A, Zheng Q. Axial helium compressor for high-temperature gas-cooled reactor: a review. Ann Nucl Energy 2019;130:54–68.
- [135] Crespi F, Gavagnin G, Sánchez D, Martínez GS. Supercritical carbon dioxide cycles for power generation: a review. Applied energy 2017;195:152–83.
- [136] Greene SR, Gehin JC, Holcomb DE, Cisneros AT, Varma VK, Corwin WR, et al. Pre-Conceptual Design of a Fluoride- Salt-Cooled Small Modular Advanced High-Temperature Reactor (SmAHTR). Tennessee. Oak Ridge National Laboratory; 2010. <https://doi.org/10.2172/1008830>.
- [137] Kuo CR, Hsu SW, Chang KH, Wang CC. Analysis of a 50 kW organic Rankine cycle system. Energy 2011;36(10):5877–85.

- [138] Quoilin S, Lemort V. Technological and economical survey of organic Rankine cycle systems. In: European conference on Economics and management of energy in industry; 2009.
- [139] Faghri A, Harley C. Transient lumped heat pipe analyses. *Heat Recovery Syst CHP* 1994;14(4):351–63.
- [140] Parand R, Rashidian B, Ataei A, Shakiby K. Modeling the transient response of the thermosyphon heat pipes. *J Appl Sci* 2009;9(8):1531–7.
- [141] Zuo ZJ, Faghri A. A network thermodynamic analysis of the heat pipe. *Int J Heat Mass Tran* 1998;41(11):1473–84.
- [142] Zhang Y, Guo K, Wang C, Tang S, Zhang D, Tian W, et al. Numerical analysis of segmented thermoelectric generators applied in the heat pipe cooled nuclear reactor. *Appl Therm Eng* 2022;204.
- [143] Cao Y, Faghri A. Transient two-dimensional compressible analysis for high-temperature heat pipes with pulsed heat input. *Numer Heat Tran* 1991;18(4): 483–502.
- [144] Chi SW. Heat pipe theory and practice: a sourcebook. 1976.
- [145] Faghri A, Buchko M. Experimental and numerical analysis of low-temperature heat pipes with multiple heat sources. 1991.
- [146] Huaiqi L, Zeyu O, Xiaoyan T, Li G, Da L, Xiaoya K, Jianqiang S. The development of high temperature heat-pipe transient model for system analysis of heat pipe cooled microreactor. *Prog Nucl Energy* 2022;146:104145.
- [147] Tian Z, Wang C, Huang J, Guo K, Zhang D, Liu X, Qiu S. Code development and analysis on the operation of liquid metal high temperature heat pipes under full condition. *Ann Nucl Energy* 2021;160:108396.
- [148] Colwell GT. Modeling of transient heat pipe operation. Atlanta (USA): Georgia Inst. of Tech.; 1987. Semiannual status report, 19 August 1986–18 February 1987 (No. N-87-27936; NASA-CR-180280; NAS-1.26: 180280).
- [149] Jang JH, Faghri A, Chang WS. Analysis of the transient compressible vapor flow in heat pipe (No. NASA-CR-185119). Cleveland, OH (United States): NASA Lewis Research Center; 1989.
- [150] Jang JH, Faghri A, Chang WS. Analysis of the one-dimensional transient compressible vapor flow in heat pipes. *Int J Heat Mass Tran* 1991;34(8):2029–37.
- [151] Issacci F, Catton I, Heiss A, Ghoniem NM. Analysis of heat pipe vapor dynamics. *Chem Eng Commun* 1989;85(1):85–94.
- [152] Hall ML, Doster JM. Transient modeling of the thermohydraulic behavior of high temperature heat pipes for space reactor applications. In: NASA-Goddard Space Flight Center, Greenbelt, Md. Fourteenth Space Simulation Conference: Testing for a Permanent Presence in Space; 1986, January.
- [153] Hall ML. Transient Thermohydraulic heat pipe modeling: incorporating THROPUT into the CESAR environment. Expanding the Frontiers of Space 2003;654:106–13.
- [154] Bowman WJ. Simulated heat-pipe vapor dynamics (friction). Air Force Institute of Technology; 1987.
- [155] Bowman WJ. Transient heat-pipe modeling-The frozen start-up problem. In: 5th Joint Thermophysics and Heat Transfer Conference; 1990. p. 1773.
- [156] Bowman WJ, Hitchcock JE. Transient, compressible heat-pipe vapor dynamics. In: ASME 1988 National Heat Transfer Conference, vol. 1; 1988. p. 329–37. vol. 1.
- [157] Faghri A. Heat pipe science and technology. Taylor & Francis; 1995.
- [158] Cao Y, Faghri A. Transient multidimensional analysis of nonconventional heat pipes with uniform and nonuniform heat distributions. 1991.
- [159] Vaartstra G, Lu Z, Lienhard JH, Wang EN. Revisiting the Schrage equation for kinetically limited evaporation and condensation. *J Heat Tran* 2022;144(8): 080802.
- [160] Lee WH. A pressure iteration scheme for two-phase flow modeling. Multiphase transport fundamentals, reactor safety, applications 1980;1:407–31.
- [161] Tan Z, Cao Z, Chu W, Wang Q. Improvement on evaporation-condensation prediction of Lee model via a temperature deviation based dynamic correction on evaporation coefficient. *Case Stud Therm Eng* 2023;48:103147.
- [162] Hall AL, Doster JM. The THROPUT code: thermohydraulic heat pipe modeling. Transactions of the Fifth Symposium on Space Nuclear Power Systems 1988, January;11:121–6.
- [163] Hall ML, Doster JM. A sensitivity study of the effects of evaporation/condensation accommodation coefficients on transient heat pipe modeling. *Int J Heat Mass Tran* 1990;33(3):465–81.
- [164] Bowman WJ. Simulated heat-pipe vapor dynamics (friction). Air Force Institute of Technology; 1987.
- [165] Tournier JM, El-Genk MS. HPTAM, a two-dimensional heat pipe transient analysis model, including the startup from a frozen state, 1.26; 1995, 199553. NAS.
- [166] Tournier JM, El-Genk MS. User's manual for HPTAM: a Two-Dimensional Heat Pipe Transient Analysis Model, Including the Startup from a Frozen State. 1995. No. NASA-CR-199552.
- [167] Tournier JM, El-Genk M. Current capabilities of "HPTAM" for modeling high-temperature heat pipes' startup from a frozen state. In: AIP conference Proceedings, vol. 608. American Institute of Physics; 2002, January. p. 139–47. 1.
- [168] Tian Z, Liu X, Wang C, Zhang D, Tian W, Qiu S, Su GH. Experimental investigation on the heat transfer performance of high-temperature potassium heat pipe for nuclear reactor. *Nucl Eng Des* 2021;378:111182.
- [169] Mahdavi M, Tiari S, De Schampheleire S, Qiu S. Experimental study of the thermal characteristics of a heat pipe. *Exp Therm Fluid Sci* 2018;93:292–304.
- [170] Jang JH, Faghri AMIR, Chang WS, Mahefkey ET. Mathematical modeling and analysis of heat pipe start-up from the frozen state. Final report. Dayton, OH (USA): Wright State Univ.; 1989 (No. N-89-28747; NASA-CR-185132; E-5028; NAS-1.26: 185132; CONF-891208-).
- [171] Tournier JM, El-Genk MS. Transient analysis of the start-up of a water heat pipe from a frozen state. *Numer Heat Tran, Part A: Applications* 1995;28(4):461–86.
- [172] Ma Y, Yu H, Huang S, Zhang Y, Liu Y, Wang C, Wang X. Effect of inclination angle on the startup of a frozen sodium heat pipe. *Appl Therm Eng* 2022;201:117625.
- [173] Sun H, Liu X, Liao H, Wang C, Zhang J, Tian W, Su GH. Experiment study on thermal behavior of a horizontal high-temperature heat pipe under motion conditions. *Ann Nucl Energy* 2022;165:108760.
- [174] Wang C, Duan Q, Liu M, Zhang D, Qiu S, Su GH, Tian W. Code development and analysis of heat pipe cooled passive residual heat removal system of Molten salt reactor. *Ann Nucl Energy* 2020;144:107527.
- [175] Zhang Z, Chai X, Wang C, Sun H, Zhang D, Tian W, Su GH. Numerical investigation on startup characteristics of high temperature heat pipe for nuclear reactor. *Nucl Eng Des* 2021;378:111180.
- [176] de Azevedo AM, dos Santos Magalhães E. The volumetric thermal capacitor method for nonlinear heat transfer in phase-change materials. *Int Commun Heat Mass Tran* 2023;142:106672.
- [177] Tournier JM, El-Genk MS. HPTAM for modeling heat and mass transfers in a heat pipe wick, during startup from a frozen state. In: AIP Conference Proceedings, vol. 324. American Institute of Physics; 1995, January. p. 123–34. 1.
- [178] El-Genk M, Tournier JM. Challenges and fundamentals of modeling heat pipes' startup from a frozen state. In: AIP conference Proceedings, vol. 608. American Institute of Physics; 2002, January. p. 127–38. 1.
- [179] Li J, Cai C, Li ZH. Knudsen diffusion differs from Fickian diffusion. *Phys Fluids* 2021;33(4).
- [180] Cao Y, Faghri A. Simulation of the early startup period of high-temperature heat pipes from the frozen state by a rarefied vapor self-diffusion model. 1993.
- [181] Tournier JM, El-Genk MS. Transient analysis of the startup of a sodium heat pipe from a frozen state. In: AIP conference proceedings, vol. 361. American Institute of Physics; 1996, March. p. 1121–8. 1.
- [182] Drioli E, Giorno L, editors. Encyclopedia of membranes. Berlin: Springer Berlin Heidelberg; 2016.
- [183] Hamila R, Chaabane R, Askri F, Jemni A, Nasrallah SB. Lattice Boltzmann method for heat transfer problems with variable thermal conductivity. *International Journal of Heat and Technology* 2017;35(2):313–24.
- [184] Grissa K, Benselama AM, Lataoui Z, Romestant C, Bertin Y, Jemni A. Performance of a cylindrical wicked heat pipe used in solar collectors: numerical approach with Lattice Boltzmann method. *Energy Convers Manag* 2017;150:623–36.
- [185] Grissa K, Benselama AM, Lataoui Z, Bertin Y, Jemni A. Investigations of the thermal performance of a cylindrical wicked heat pipe. *Int J Energy Res* 2018;42 (9):3048–58.
- [186] Liu D, Wang X, He Y. Lattice Boltzmann simulation of flow in random porous media constructed by quartet structure generation set. *J Eng Thermophys* 2021; 42(1):210–4.
- [187] Chen HX, Guo YX, Yuan DZ, Ji Y. Experimental study on frozen startup and heat transfer characteristics of a cesium heat pipe under horizontal state. *Int J Heat Mass Tran* 2022;183:122105.
- [188] Dussinger PM, Anderson WG, Sunada ET. Design and testing of titanium/cesium and titanium/potassium heat pipes. Proceedings of the 2005 IECEC 2005;AIAA: 15–8.
- [189] Reid RS, Sena JT, Nehrbauer JP. Sodium compatibility tests of MA-ODS 754 and MA-ODS 956 alloys. In: AIP conference proceedings, vol. 746. American Institute of Physics; 2005, February. p. 164–70. 1.
- [190] Manoj R, Kumar M, Narasimha Rao R, Rama Narasimha K, Suresh PVS. Performance evaluation of sodium heat pipe through parameteric studies. *Frontiers in Heat Pipes (FHP)* 2013;3(4).
- [191] Lee BI, Lee SH. Manufacturing and temperature measurements of a sodium heat pipe. *KSME Int J* 2001;15:1533–40.
- [192] Wang C, Liu X, Liu M, Tang S, Tian Z, Zhang D, Su GH. Experimental study on heat transfer limit of high temperature potassium heat pipe for advanced reactors. *Ann Nucl Energy* 2021;151:107935.
- [193] Zhang H, Ye F, Guo H, Yan X. Sodium-potassium alloy heat pipe under geyser boiling experimental study: heat transfer analysis. *Energies* 2021;14(22):7582.
- [194] Huang PH, Ahn T, Manera A, Petrov V. Investigation of key parameters for the operation of a sodium heat pipe with visualization using X-ray radiography. *Appl Therm Eng* 2024;236:121867.
- [195] Chen HX, Guo YX, Yuan DZ, Ji Y. Thermal performance of a medium temperature cesium heat pipe at different inclination angles. *Int Commun Heat Mass Tran* 2022;138:106363.
- [196] Tian Z, Zhang J, Wang C, Guo K, Liu Y, Zhang D, Su GH. Experimental evaluation on heat transfer limits of sodium heat pipe with screen mesh for nuclear reactor system. *Appl Therm Eng* 2022;209:118296.
- [197] Ma Y, Yu H, Huang S, Zhang Y, Liu Y, Wang C, Wang X. Effect of inclination angle on the startup of a frozen sodium heat pipe. *Appl Therm Eng* 2022;201:117625.
- [198] Guo Q, Guo H, Yan XK, Ye F, Ma CF. Influence of inclination angle on the start-up performance of a sodium-potassium alloy heat pipe. *Heat Transf Eng* 2018;39 (17–18):1627–35.
- [199] Wang C, Zhang L, Liu X, Tang S, Qiu S, Su GH. Experimental study on startup performance of high temperature potassium heat pipe at different inclination angles and input powers for nuclear reactor application. *Ann Nucl Energy* 2020; 136:107051.
- [200] Ma Z, Wu Q, Ma Y, Tang S, Zhang L, Liu C, Pan L. The nucleation characteristics of geyser boiling in sodium heat pipes. *Ann Nucl Energy* 2025;211:111010.
- [201] Kwart SM, Kumar R, Moreno G, Yoo J, You SM. Pool boiling characteristics of low concentration nanofluids. *Int J Heat Mass Tran* 2010;53(5–6):972–81.
- [202] Shahmoradi Z, Etesami N, Esfahany MN. Pool boiling characteristics of nanofluid on flat plate based on heater surface analysis. *Int Commun Heat Mass Tran* 2013; 47:113–20.

- [203] Sheikhbahai M, Esfahany MN, Etesami N. Experimental investigation of pool boiling of Fe304/ethylene glycol–water nanofluid in electric field. *Int J Therm Sci* 2012;62:149–53.
- [204] Ahmed O, Hamed MS. Experimental investigation of the effect of particle deposition on pool boiling of nanofluids. *Int J Heat Mass Tran* 2012;55(13–14): 3423–36.
- [205] Liu ZH, Liao L. Sorption and agglutination phenomenon of nanofluids on a plain heating surface during pool boiling. *Int J Heat Mass Tran* 2008;51(9–10): 2593–602.
- [206] Coursey JS, Kim J. Nanofluid boiling: the effect of surface wettability. *Int J Heat Fluid Flow* 2008;29(6):1577–85.
- [207] Huang CK, Lee CW, Wang CK. Boiling enhancement by TiO₂ nanoparticle deposition. *Int J Heat Mass Tran* 2011;54(23–24):4895–903.
- [208] Kim HD, Kim J, Kim MH. Experimental studies on CHF characteristics of nanofluids at pool boiling. *Int J Multiphas Flow* 2007;33(7):691–706.
- [209] Kim HD, Kim MH. Effect of nanoparticle deposition on capillary wicking that influences the critical heat flux in nanofluids. *Appl Phys Lett* 2007;91(1).
- [210] Edel Z, Mukherjee A. Flow boiling dynamics of water and nanofluids in a single microchannel at different heat fluxes. *J Heat Tran* 2015;137(1):011501.
- [211] Yu L, Sur A, Liu D. Flow boiling heat transfer and two-phase flow instability of nanofluids in a minichannel. *J Heat Tran* 2015;137(5):051502.
- [212] Arya A, Sarafraz MM, Shahmiri S, Madani SAH, Nikkhah V, Nakhjavani SM. Thermal performance analysis of a flat heat pipe working with carbon nanotube–water nanofluid for cooling of a high heat flux heater. *Heat Mass Tran* 2018;54: 985–97.
- [213] Tsai CY, Chien HT, Ding PP, Chan B, Luh TY, Chen PH. Effect of structural character of gold nanoparticles in nanofluid on heat pipe thermal performance. *Mater Lett* 2004;58(9):1461–5.
- [214] Wang GS, Song B, Liu ZH. Operation characteristics of cylindrical miniature grooved heat pipe using aqueous CuO nanofluids. *Exp Therm Fluid Sci* 2010;34(8):1415–21.
- [215] Moraveji MK, Razvarz S. Experimental investigation of aluminum oxide nanofluid on heat pipe thermal performance. *Int Commun Heat Mass Tran* 2012;39(9): 1444–8.
- [216] Zhou Y, Yang H, Liu L, Zhang M, Wang Y, Zhang Y, Zhou B. Enhancement of start-up and thermal performance in pulsating heat pipe with GO/water nanofluid. *Powder Technol* 2021;384:414–22.
- [217] Gupta NK, Tiwari AK, Ghosh SK. Experimental study of thermal performance of nanofluid-filled and nanoparticles-coated mesh wick heat pipes. *J Heat Tran* 2018;140(10):102403.
- [218] Tharayil T, Godson Asirvatham L, Rajesh S, Wongwises S. Effect of nanoparticle coating on the performance of a miniature loop heat pipe for electronics cooling applications. *J Heat Tran* 2018;140(2):022401.
- [219] Jyothi Sankar PR, Venkatachalam S, Santhosh Kumar MC. Effect of hydrophilic coating on mesh wicks used in heat pipes. *Surf Eng* 2020;36(7): 680–6.
- [220] Zohuri B. Nuclear micro reactors. Cham Switzerland: Springer International Publishing; 2020.
- [221] Zhang Y, Guo K, Wang C, Zhang J, Wang Y, Tian W, Qiu S. Artificial neural network for geometric design and optimization of three-stage segmented thermoelectric generators. *Appl Therm Eng* 2024;124077.
- [222] Panxiao LI, Zhipeng ZHANG, Zhiwen DAI, Chenglong WANG, Wenxi TIAN, Suizheng QIU, Guanghui SU. Conceptual design and demonstration test of dual-mode heat pipe reactor prototype. *Atomic Energy Sci Technol* 2023;57(1):66–73.
- [223] Poston DI, Gibson MA, Godfroy T, McClure PR. KRUSTY reactor design. *Nucl Technol* 2020;206(sup1):S13–30.
- [224] Poston DI, McClure PR. From DUFF to KRUSTY—the path to Successful Reactor Development [Slides] (No. LA-UR-20-27613). Los Alamos, NM (United States): Los Alamos National Laboratory (LANL); 2020.
- [225] Poston DI, Godfroy T, McClure PR, Sanchez RG. KiloPower project-KRUSTY experiment nuclear design (No. LA-UR-15-25540). Los Alamos, NM (United States): Los Alamos National Laboratory (LANL); 2015.
- [226] McClure PR, Poston DI, Clement SD, Restrepo L, Miller R, Negrete M. KRUSTY experiment: Reactivity insertion accident analysis. *Nucl Technol* 2020;206(sup1): S43–55.
- [227] Tang S, Wang C, Liu X, Su G, Tian W, Qiu S, Bai S. Experimental investigation of a novel heat pipe thermoelectric generator for waste heat recovery and electricity generation. *Int J Energy Res* 2020;44(9):7450–63.
- [228] Guo K, Zhang Y, Lin X, Huang J, Wang C, Qiu S, Su G. Transient thermoelectric characteristics of the principle prototype for the heat pipe cooled nuclear Silent thermoelectric reactor (NUSTER). *Ann Nucl Energy* 2023;189:109818.
- [229] Huang J, Wang C, Guo K, Zhang D, Su GH, Tian W, Qiu S. Heat transfer analysis of heat pipe cooled device with thermoelectric generator for nuclear power application. *Nucl Eng Des* 2022;390:111652.
- [230] Zhang Y, Chai X, Wang C, Tang S, Zhang D, Tian W, Qiu S. Thermal-hydraulic analysis of heat pipe reactor experimental device with thermoelectric generators. *Prog Nucl Energy* 2022;146:104137.
- [231] Wang Z, Zhang M, Gou J, Xu S, Shan J. Study on start-up characteristics of a heat pipe cooled reactor coupled with a supercritical CO₂ Brayton cycle. *Appl Therm Eng* 2024;236:121893.
- [232] Jahanfarinia G, Zarifi E. Thermodynamic simulation of supercritical carbon dioxide brayton cycle in an advanced nuclear power plant equipped with a heat pipe cooled microreactor. *Iran. J. Chem. Chem. Eng.(IJCCE) Research Article* 2024;43(5).
- [233] Lee SW, Lee Y, Kim N, Jo H. Design of heat pipe cooled microreactor based on cycle analysis and evaluation of applicability for remote regions. *Energy Convers Manag* 2023;288:117126.
- [234] Romano LF, Ribeiro GB. Optimization of a heat pipe-radiator assembly coupled to a recuperated closed Brayton cycle for compact space power plants. *Appl Therm Eng* 2021;196:117355.
- [235] Li J, Hu Z, Jiang H, Guo Y, Li Z, Zhuge W, Ouyang M. Coupled characteristics and performance of heat pipe cooled reactor with closed Brayton cycle. *Energy* 2023; 280:128166.
- [236] Deng J, Guan C, Wang T, Liu X, Chai X. Evaluation of start-up characteristics for heat pipe-cooled nuclear reactor coupled with recuperated open-air brayton cycle using hardware-in-the-loop. *Energy* 2024;301:131698.
- [237] Tu ST, Zhang H, Zhou WW. Corrosion failures of high temperature heat pipes. *Eng Fail Anal* 1999;6(6):363–70.
- [238] Ewell G, Basilius A, Lamp T. Reliability of low-cost liquid metal heat pipes. In: 3rd international Heat Pipe Conference; 1978, May. p. 437.
- [239] Chen Z, Zou D. Accelerated service life testing and analysis of heat pipe for high temperature. *Journal of Iron and Steel Research* 1986;6(2):79–84.
- [240] Tu S, Zhang H, Zhuang J. The strength and life of heat pipe equipment. *Press Vessel Technol* 1997;14(2):30–7, 90.
- [241] Jin F, Song H. Development of porous isothermal sodium heat pipe for high temperature. *Control Eng China* 1986;2:1–5.
- [242] Clark AJ. Failures and Implications of heat pipe systems (No. SAND2019-11808). Albuquerque, NM (United States): Sandia National Lab.(SNL-NM); 2019.
- [243] Lee DH, Bang IC. Dry-out limit enhancement strategy in sodium heat pipes: Overfilling effect and modified capillary limit model. *Int J Heat Mass Tran* 2024; 228:125633.
- [244] Zhang M, Miao Q, Zhang S, Ma Y, Ding S, Zhang Z, Gu Z. Experimental study of non-condensable gas effects on sonic limit of sodium heat pipe. *Appl Therm Eng* 2023;232:120970.
- [245] Ma Y, Zhang Y, Yu H, Su GH, Huang S, Deng J, Zhang Z. Capillary evaporating film model for a screen-wick heat pipe. *Appl Therm Eng* 2023;225:120155.
- [246] Ma Y, Yu H, Wang X, Zhang Y, Huang S, Wang C, Chai X. Experimental study on sodium Screen-Wick heat pipe capillary limit. *Appl Therm Eng* 2023;227:120397.
- [247] Nilsson KF, Dolci F, Seldis T, Ripplinger S, Grah A, Simonovski I. Assessment of thermal fatigue life for 316L and P91 pipe components at elevated temperatures. *Eng Fract Mech* 2016;168:73–91.
- [248] Kim WG, Kim SH, Ryu WS. Evaluation of Monkman-Grant parameters for type 316LN and modified 9Cr-Mo stainless steels. *KSME Int J* 2002;16:1420–7.
- [249] Jones DL. Time-temperature relationships in stress rupture and creep of metals and alloys. In: Strength of metals and alloys (ICMSA 8). Pergamon; 1989. p. 953–8.
- [250] Wang D, Ma Y, Hong F. Three-dimensional CFD simulation of geyser boiling in high-temperature sodium heat pipe. *Nucl Eng Technol* 2024;56(6):2029–38.
- [251] Ma Y, Han W, xie B, Yu H, Liu M, He X, Chai X. Coupled neutronic, thermal-mechanical and heat pipe analysis of a heat pipe cooled reactor. *Nucl Eng Des* 2021;384:111473.
- [252] Li T, Xiong J, Xie Q, Chai X. Performance analysis of heat pipe micro-reactor with Stirling engine based on full-scope multi-physics coupled simulation. *Energy* 2024;134011.
- [253] Wang Y, Ma Y, Jiang N. Steady state neutronic and thermal-mechanical coupling analysis of inelastic deformation in solid-state heat pipe cooled reactor. *Ann Nucl Energy* 2024;208:110802.
- [254] Zhang J, Li T, Shen Z, Li X, Xiong J, Chai X, Zhang T. Investigations of multiphysics models on a megawatt-level heat pipe nuclear reactor based on high-fidelity approaches. *Nucl Sci Eng* 2024;198(5):1097–121.
- [255] Ma Y, Chen E, Yu H, Zhong R, Deng J, Chai X, Zhang Z. Heat pipe failure accident analysis in megawatt heat pipe cooled reactor. *Ann Nucl Energy* 2020;149: 107755.
- [256] Ma Y, Liu J, Yu H, Tian C, Huang S, Deng J, He X. Coupled irradiation-thermal-mechanical analysis of the solid-state core in a heat pipe cooled reactor. *Nucl Eng Technol* 2022;54(6):2094–106.
- [257] Lee C, Jung YS. Development of the PROTEUS and ANSYS coupled system for simulating Heat Pipe Cooled Micro Reactors (No. ANL/NSE-20/4). Argonne, IL (United States): Argonne National Lab. (ANL); 2020.
- [258] Guo Y, Li Z, Huang S, Liu M, Wang K. A new neutronics-thermal-mechanics multiphysics coupling method for heat pipe cooled reactor based on RMC and OpenFOAM. *Prog Nucl Energy* 2021;139:103842.
- [259] Guo Y, Li Z, Wang K, Su Z. A transient multiphysics coupling method based on OpenFOAM for heat pipe cooled reactors. *Sci China Technol Sci* 2022;65(1): 102–14.
- [260] Jeong MJ, Im J, Lee S, Cho HK. Multiphysics analysis of heat pipe cooled microreactor core with adjusted heat sink temperature for thermal stress reduction using OpenFOAM coupled with neutronics and heat pipe code. *Front Energy Res* 2023;11:1213000.
- [261] Xiao W, Li X, Li P, Zhang T, Liu X. High-fidelity multi-physics coupling study on advanced heat pipe reactor. *Comput Phys Commun* 2022;270:108152.
- [262] Wu A, Wang W, Zhang K, Shen S, Duan W, Pan R, Chen H. Multiphysics coupling analysis of heat pipe reactor based on OpenMC and COMSOL Multiphysics. *Ann Nucl Energy* 2023;194:110115.

- [263] Chen H, Wang W, Wu A, Zhang K, Pan R, Duan W, Luo X. Multi-physics coupling analysis of test heat pipe reactor KRUSTY based on MOOSE framework. Nucl Eng Des 2023;414:112597.
- [264] Matthews C, Laboure V, DeHart M, Hansel J, Andrs D, Wang Y, Martineau RC. Coupled multiphysics simulations of heat pipe microreactors using DireWolf. Nucl Technol 2021;207(7):1142–62.
- [265] Stauff N, Abdelhameed A, Cao Y, Fassino N, Ibarra L, Miao Y, Nunez D. High-fidelity multiphysics load following and accidental transient modeling of microreactors using NEAMS tools: Application of NEAMS codes to perform multiphysics modeling analyses of micro-reactor concepts (No. ANL/NEAMS-23/4). Argonne, IL (United States): Argonne National Laboratory (ANL); 2023.